The Journal of Acoustical Society of India
Volume 49 Number 1-2 January 2022 pp 1-47

ISSN 0973-3302

THE JOURNAL OF ACOUSTICAL SOCIETY OF INDIA

Volume 49 Number 1-2 January 2022

A Quarterly Publication of the ASI
https://acoustics.org.in

The Journal of Acoustical Society of India

The Refereed Journal of the Acoustical Society of India (JASI)

The Journal of Acoustical Society of India is a refereed journal of the Acoustical Society of India **(ASI)**. The **ASI** is a non-profit national society founded in 31st July, 1971. The primary objective of the society is to advance the science of acoustics by creating an organization that is responsive to the needs of scientists and engineers concerned with acoustics problems all around the world.

Manuscripts of articles, technical notes and letter to the editor should be submitted to the Chief Editor. Copies of articles on specific topics listed above should also be submitted to the respective Associate Scientific Editor. Manuscripts are refereed by at least two referees and are reviewed by Publication Committee (all editors) before acceptance. On acceptance, revised articles with the text and figures scanned as separate files on a diskette should be submitted to the Editor by express mail. Manuscripts of articles must be prepared in strict accordance with the author instructions.

All information concerning subscription, new books, journals, conferences, etc. should be submitted to Chief Editor:

B. Chakraborty, CSIR - National Institute of Oceanography, Dona Paula, Goa-403 004,
Tel: +91.832.2450.318, Fax: +91.832.2450.602, e-mail: bishwajit@nio.org

Annual subscription price including mail postage is Rs. 2500/= for institutions, companies and libraries and Rs. 2500/= for individuals who are not **ASI** members. The Journal of Acoustical Society of India will be sent to **ASI** members free of any extra charge. Requests for specimen copies and claims for missing issues as well as address changes should be sent to the Editorial Office:

ASI Secretariat, C/o Acoustics and Vibration Metrology, CSIR-National Physical Laboratory, Dr. KS Krishnan Road, New Delhi 110 012, Tel: +91.11.4560.8317, Fax: +91.11.4560.9310, e-mail: asisecretariat.india@gmail.com

ISSN 0973-3302

Printed at Alpha Printers, WZ-35/C, Naraina, Near Ring Road, New Delhi-110028 Tel.: 9810804196. JASI is sent to ASI members free of charge.

The Journal of Acoustical Society of India

A quarterly publication of the Acoustical Society of India

Volume 49, Number 1-2, January 2022

ARTICLES

INFORMATION

The Journal of Acoustical Society of India : Vol. 49, No. 1-2, 2022 (pp. 1-11)

Shallow water soundscape off-Goa Grande Island

Kranthikumar Chanda and Bishwajit Chakraborty
CSIR-National Institute of Oceanography, Dona Paula, Goa-403 004, India
e-mail: bishwajit.chakraborty837@gmail.com

[Received: 28-12-2021; Accepted: 25-01-2022]

ABSTRACT

Soundscape monitoring is an effective tool to characterize Marine habitats. The passive acoustic studies lead to an understanding of the biodiversity of the ecosystem. Analyses of the soundscape data acquired at 30m water depth are carried out along with the kind of anthropogenic sound. An algorithm to segment the recorded data is described. We identified that the recorded fish sound from Grande Island is similar to the species Condon nobilis (also known as a Barred grunt) of the Haemulidae family, which is commonly available in the western Atlantic. However, such species are not reported from the present area. Four species types of the Haemulidae family are reported from the Grande Island area using gillnet fishing. The available information and acquired sound data suggest that fish sound data belongs to the Haemulidae family though more investigation is needed to identify the species.

1. INTRODUCTION

Hydroacoustic is the science of sound waves in the water that has become an important tool for underwater remote sensing (Balk, 2001; Shabangu *et al.,* 2014). Hydroacoustic can be broadly classified as two disciplines: *(i)* active and *(ii)* passive acoustics. For an active acoustic system, acoustic pulses are transmitted into the water for producing backscatter echoes. By examining the received echoes, it is possible to estimate the range and in certain cases detecting the presence and bearing of an underwater target (Urick, 1983). Active acoustic systems are widely used for many oceanographic applications (Mann *et al.,* 2008). However, the transmission of sound levels in the ocean for a prolonged duration may cause long-range effects on aquatic animal health (Popper and Hawkins, 2012). Active acoustic activities (for *e.g.,* in marine protected areas) are now being subject to formal permission as emerged recently (Tyack *et al.,* 2015). Therefore, passive acoustic technique, a method for detecting and monitoring acoustic signals in an underwater environment is advancing as a vital tool for ocean soundscape studies.

The passive acoustic system transmits no signal, and it is designed to detect acoustic signals emanating from the original sources, including natural processes in the ocean, underwater noise sources of biological origin such as marine mammals (Southhall *et. al.,* 2007), crustaceans or fish (Tavolga, 1971) and anthropogenic noise sources (Ainslie, 2012). By analyzing passive acoustic recordings, it is possible to discriminate and identify different animal species and to calculate the relative number of animals present within the measurement range. These key pieces of information can be complemented by ocean productivity or yearly migratory passage of animals such as great whales. A new application of passive acoustics involves awareness of environmental issues, which has spurred the development of passive acoustic techniques (Nystuen *et al.,* 2004). Progress in the field of passive acoustics has attracted researchers to investigate physical and biological processes such as oceanic features, seafloor habitats, and associated processes (Dahl *et al.,* 2007). There is a growing consensus that anthropogenic sound levels in oceans are increasing that can have adverse effects on marine life (Tyack, 2008).

Hitherto, most of the passive acoustic experiments such as propagation modeling and related geo-acoustic inversion studies have been carried out in deeper waters (Gervaise *et al.,* 2007). However, the focus is needed for shallow water studies such as physical and biological characterization of a littoral environment (Pace and Jensen, 2002), especially in the reef and off reef regions (Bertucci *et al.,* 2016). Understanding the underwater environment is possible through ambient sound field measurement and "soundscape" studies (Pijanowski *et. al.,* 2011). The term "soundscape" has been used in many disciplines to describe the relationship between the waterscape (or landscape) and the relative composition of sound present.

Most of the fishes and invertebrates use sound for vital life functions. Based on a review of 115 primary studies encompassing various human-produced underwater noise sources, 66 species of fish and 36 species of invertebrates reveal noise impacts on development, including body malformations, higher egg or immature mortality, developmental delays, delays in metamorphosing and settling, and slower growth rates (Weilgart, 2018). Anatomical impacts from noise involve massive internal injuries, cellular damage, hearing loss, and even mortality (Hastings and Popper, 1996; Hawkins and Poppers, 2017). Ecological functions of invertebrates such as water filtration, mixing sediment layers, and bio-irrigation, which are key to nutrient cycling on the seabed, were adversely affected by noise. Once the population biology and ecology are impacted, it will have succeeding consequences on fisheries and even food security for humans.

Studies on population dynamics and related ecosystem function of non-migratory fishes and invertebrates are relatively easy to accomplish as compared to migratory marine mammal species. Many fish species rely on vocal signaling during their activities and produce sounds using sonic muscles that vibrate the swimbladder or bony elements (stridulation) (Fine and Parmentier, 2015; Permentier *et al.,* 2016). Fishes use sound to attract mates and defend their territory (Vasconcelos *et al.,* 2010). In shallow water, the ambient sound field generally consists of various types of sound sources such as fish sounds (biophonies), wind and flow sounds (geophony), and boat sounds (anthrophony) (McWilliam and Hawkins, 2013). The spatial structure of the sound field is dependent on the nature of the waveguide comprising the multipath sound propagation between the sea surface and the seabed (Jensen *et al.,* 2011). Therefore, the characteristics of any signal received at the recording location can be affected by the variability of environmental parameters (*i.e.,* sound speed and absorption) in the medium. If these propagation features are characterized, it is possible to use the recorded soundscape and fish sound as an acoustic metric for studying ecosystem function (Rountree *et al.,* 2006).

In this context, the analysis presented here expounds passive acoustic (fish sound) data recorded using an autonomous wideband hydrophone system with an intention to understand shallow-water biodiversity of the study area (Au and Lammers, 2016). In general, the temporal and spectral characteristics of passive acoustic recordings such as "oscillogram", "spectrogram", and peak sound level of the "power spectral density" (PSD) are used for fish sound identification (Fish and Mowbray, 1970; Erbe *et al.,* 2015; McCauley and Cato, 2000; Mahanty *et al.,* 2015). The power spectrum encompasses several dominant frequencies, which presumably represent major oscillation modes in the fish sound, but the amplitudes of these modes vary in a complex manner (Wilden *et al.,* 1998; Chakraborty *et al.,* 2014; Chanda *et al.,* 2020a; Chanda *et al.,* 2020b). Here, we present soundscape of the Grande Island off Goa location having water depth of 30m.

2. METHODOLOGY

2.1 Materials and methods

Here, investigations making use of passive acoustic data is carried out. For this purpose, the Song

Meter acoustic system for a marine application is extensively used for fish sound data acquisition. Present work illustrates how the passive acoustic data were acquired employing Song Meter (SM2M+). Acquisition of ancillary data such as wind, current, water temperature, sound velocity profiler data as well as surface sediment data is also a component of data acquisition. Here, the technical aspect of the Song Meter system is discussed.

2.2 *Song meter*

The Song Meter acoustic system (https://www.wildlifeacoustics.com) is a cost-effective, weatherproof marine recorder that can be used for underwater acoustic monitoring of fish. It has also been effectively used during long-term bioacoustics monitoring of dolphins, whales and other marine life including fish as well as and anthropogenic noise in an underwater environment. Song Meter systems, SM2M+ is used for present data acquisition activities. This recorder (SM2M+), is submersibles having a 16-bit analog to digital converter designed for short- or long-term deployment in fresh or saltwater. The unit is designed to allow quick refurbishment of the device along shipside for immediate redeployment. The batteries and SD flashcards can be easily swapped and the housing resealed for redeployment. The device can be anchored and recovered via tether, diver or by optional acoustic release. These systems are self-buoyant submersible that uses a thick-walled PVC housing rated for deployment up to a depth of 150 m. The core electronic motherboard accommodates 32 D cell batteries which are installed on both sides of the board. Dimension wise, the system (SM2M+) is identically cylindrical shaped with a height 79.4 cm and 16.5 cm diameter, they can be fitted with a hydrophone with a length of 2.5 cm and 1.9 cm diameter. The systems weigh around 9.5 kg in the air without batteries, and the buoyancy in saltwater is 5.5 kg.

The SM2M+ system consists of a single hydrophone having a frequency bandwidth of 2 Hz - 48 kHz. The system records in audio (WAV) format files for predefined sampling interval. The sensitivity of the hydrophone is calibrated to 0.1 dB resolution. The SM2M+ submersible is powered through 32 D cells alkaline batteries. The recorder can accept 1.5V alkaline batteries, 1.2V NiMH batteries or 3V-3.3V lithium batteries. A board contains protection diodes that must be configured for the appropriate cell voltage. The SM2M+ is normally configured for 1.5 or 1.2 V cells. In this configuration the batteries are wired in parallel groups of 4 in series. Two AA batteries run the SM2M+ clock. The system has the battery life and memory capacity to record for hundreds of hours. The Song Meter systems were calibrated at ESSO-National Institute of Ocean Technology (NIOT) calibration facility (http://www.niot.res.in/ATF/). Operational deployment of SM2M+ and SM3M including schematic diagram of the mooring system is displayed (Fig. 1) along with the deployment photographs of the Song Meter (SM2M+).

2.3 *Study area*

In this work, passive acoustic data were acquired from new regions of the Grande Island from WCI (Western Continental Shelf of India). The area is located at relatively deeper than the previous study areas (Chanda *et al.,* 2020a; Chanda *et al.,* 2020b; Chanda *et al.,* 2020c). Passive acoustic data along with the ancillary data were acquired from Grande Island, acquisitions of fish sound data at spot locations. The data recorded (8-12 May 2015) from the deeper part at 30m water depth (Location 4: 15°18.544' N 73°41.667' E) are used for fish sound analyses. Fish identification studies utilizing fish sound analyses are presented here.

2.4 *Spectral methods*

In this section spectral techniques such as spectrogram for visualization of segmented fish sound data is made. Similarly, power spectral density is applied to estimate the frequency peak of the fish calls and for the identification of fish calls. Here, these two techniques are extensively used.

Spectrogram : It provides the time localized frequency information for situations in which frequency components of a signal vary over time. The spectrogram is a visualization of time series to understand the frequency pattern of the recorded signal. The spectrogram is a linear time-frequency representation of the pre-windowing of the fish sound signal, and calculating its Fourier transform. This transform is

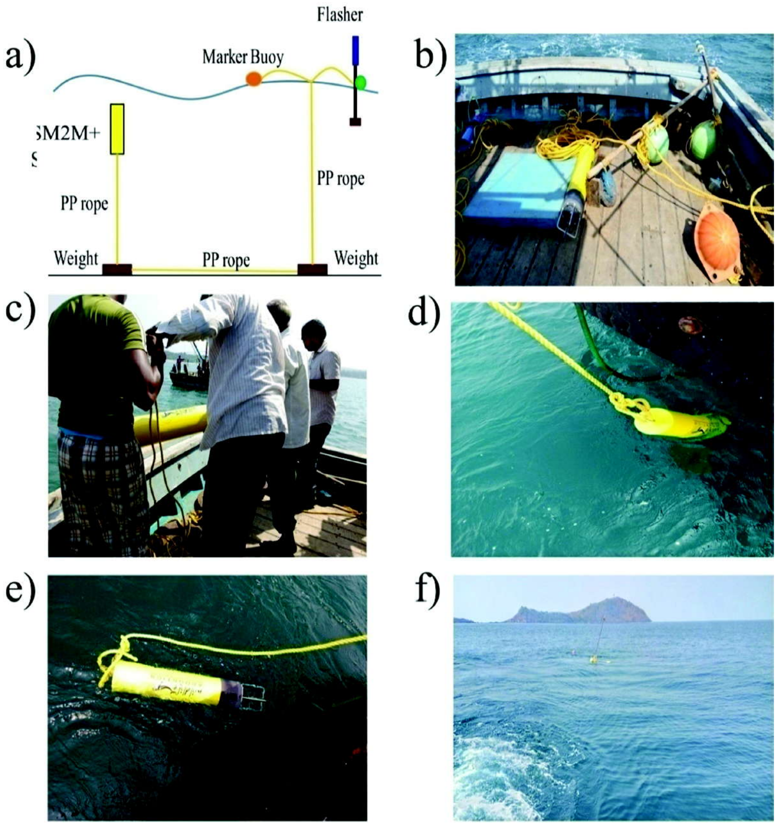

Fig. 1. Operational deployment of SM2M+ and SM3M: **(a)** schematic diagram of the mooring system is given along with the deployment photographs of the Song Meter (SM2M+ and SM3M). **(b-f).** The Song Meter system is programmed at the shore to finalize the data acquisition timings. The equipment is synchronized with the current meter where acoustic Doppler technique is used. This is necessary to avoid recording acoustic signal emanating from ADCP based current meter. U shaped moorings having positively buoyant Song Meter submersible (SM2M+) tied to a 40 kg dead weight, which is lying on the seafloor, is employed here. The same deadweight is tied to another deadweight which is lying on the seafloor by a twenty-meter long rope. 2-3 glass floats where each float weighs around 20 kg to another mooring where beacon lights are attached to the floats to maintain the lights above the surface are used. For the Song Meter system, beacon light is important from the safety and navigational aspects.

known as a Short Time-Fourier Transform and referred to as STFT *(t, f)* where t is the time variable and f the frequency. A quadratic form related to the Short Time Fourier Transform can be obtained by taking the square of this transform. The spectrograms provide the spectral energy density of the signal in the time-frequency domain. The spectrogram of a signal *x(t)* is referred to as SPECT *(t, f)* (Padovese *et al.*, 2009)

$$\mathrm{SPECT}(t, f) = \left| \int x(\tau)\, h^*(\tau - t) e^{-2j\pi f\tau}\, d\tau \right|^2 \tag{1}$$

where *h(t)* is a sliding window weight, and the superscript * denotes conjugate. Matlab (www. mathwork.com) was employed.

Power Spectral Density (PSD) : Power spectral density is the measure of signal power content versus frequency. The power spectral density is typically used to characterize the peak frequency of the signal. The power spectrum is defined as the square of the amplitude of the Fourier transform of a time series and can thus be regarded as an expression of the variance of the underlying process. Power spectral density function (PSD) shows the strength of the variations (energy) as a function of frequency. In other words, it shows at which frequencies variations are strong and at which frequencies variations are weak. The unit of PSD is energy per frequency (width) and energy can be obtained within a specific frequency range by integrating PSD within that frequency range. Computation of PSD is done directly by the method called FFT or computing autocorrelation function and then transforming it.

2.5 *Spectral analyses*

Spectral analyses of 1 to 2 minutes of data acquired at the 15-minute interval were used to calculate power spectral density (PSD). Concatenated PSDs were generated on the time-frequency axis for location soundscape. Such soundscape plots indicating the duration of data acquisition, and intensity depicted by the color bar are presented. Thereafter, the recorded sounds were analyzed using an algorithm developed for the purpose (Fig. 2), waveforms, spectrograms and power spectral density (PSD) applied to the segmented signals of individual fish calls (Fig. 3). Spectrograms visualize the time-frequency content of the signal, and are commonly used to analyze animal vocalizations. More details of animal vocalization have been covered in this chapter. PSD has been used to estimate peak frequency. For estimation of the PSD and spectrogram, Matlab (www. mathwork.com) related functions were used. Furthermore, temporal call parameters such as call duration, the number of pulses and inter-cell separation of the fish calls were made use of to identify the fish sound. In order to corroborate the fish sounds, available data of fish sound files accessible on the websites *(i)* Discovery of Sound in the Sea (https://dosits.org/galleries/audio-gallery/#fish), *(ii)* The Fish Base project (http://www.fishbase.org/) and *(iii)* Mc Cauley library (https://m.soundcloud.com/abc-science/sounds-of-science-teraponsspawning) were utilized. Besides, the seminal work on biological underwater sounds for fish sound identification (Fish and Mowbray, 1970) was extensively made use of.

3. RESULTS AND DISCUSSION

For identification of the fish species, calculations for estimation of the spectrograms and PSDs of an individual call are made. For spectrogram, the 'pwelch' function is used. For species identification, temporal and spectral parameters of the fish calls are determined (Fish and Mowbray, 1970). The inter-call interval (from the end of one call to start of next call), single call duration and the number of pulses per bout were estimated. The spectral parameters such as PSD of single call are also calculated using 'pwelch' function, and the frequency peaks are estimated.

The procedure to determine fish sound parameters requires noise reduction, segmentation and classification (Chanda *et al.,* 2020a). Therefore, to understand the nature of the biological sound present, the spectrogram (b in Fig. 2), of the raw 60 sec data is generated. A large spurt of signals is observed close to the lower frequencies. The PSD of the entire data has been depicted [Fig. 2 (c)]. Thereafter, an application of the noise reduction method is employed (Zimmer, 2011). The extraction of noise-free fish sound is imperative before data processing. In order to identify the start and stop point of the individual fish call, an enhancement of the contrast between signal and background noise in the data stream is required. Therefore, noise level reduction is carried out by multiplying the time series with ratios of its corresponding absolute to the maximum absolute value (d in Fig. 2) (Haris *et al.,* 2014). In the next step, Hilbert transform based envelope detection procedure is applied. Data segmentation is implemented in two steps. At first the coarse segmenting each call is visually completed. Next, a cumulative sum is employed across the individual data to determine the exact start and stop time. A sharp rise in the slope of the cumulative sum marks the beginning of a sound event. The flat or saturated part of the curve corresponds to the end of a sound event (e & f in Fig. 2). After segmenting the signals, to identify the fish family/species, the spectrogram of each call signal is generated (g in Fig. 2). Each fish family/species produces a sound that will have a peak frequency which is distinct, and can be used to distinguish the species. To determine the peak frequency, the PSD plots of all the call signals, (h in Fig. 2), are compared with the peak frequencies of the segmented call signal and those given in the referenced works. Thereafter, the determination of temporal parameters such as call duration, number of pulses within the calls, and inter-call durations are made. Detailed temporal and spectral parameters are shown (Fig. 3):

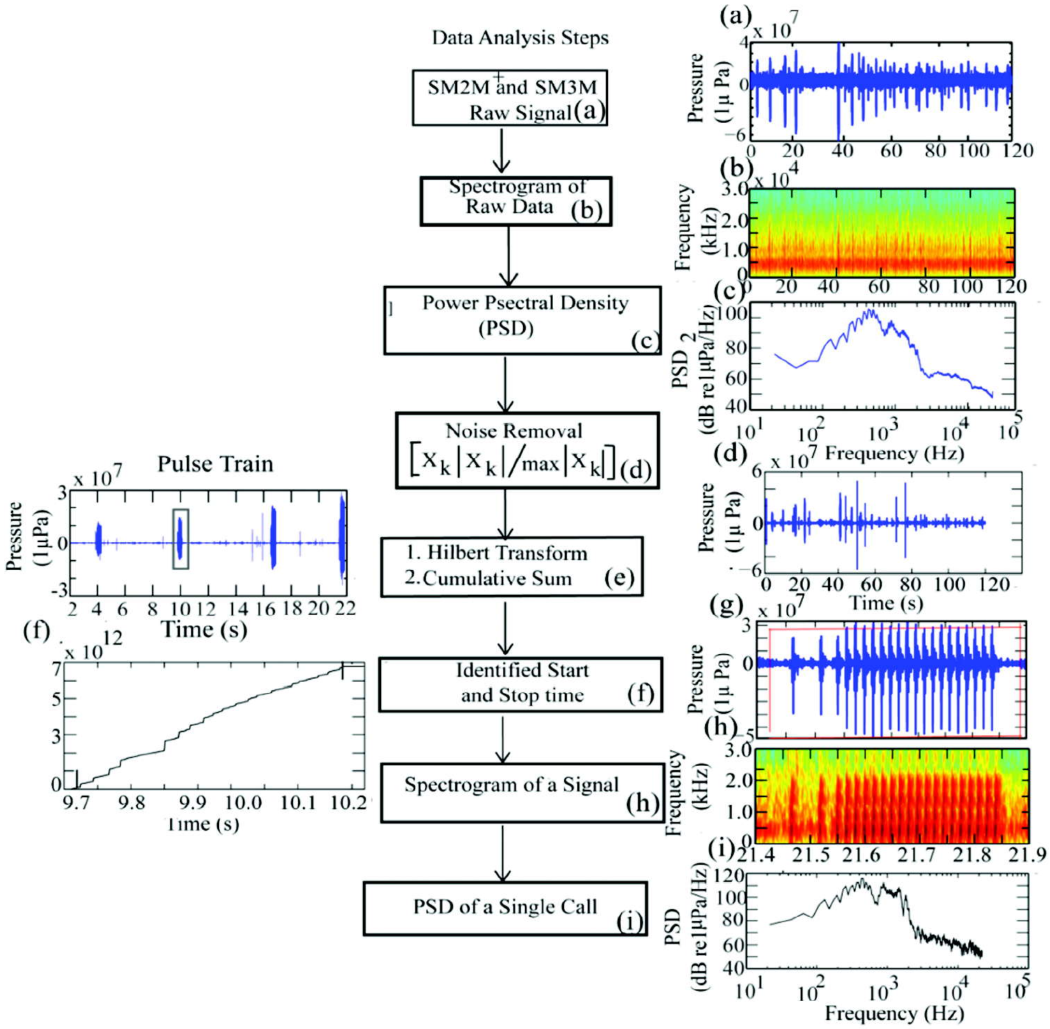

Fig. 2. Fish sound segmentation technique flow chart employed in this work (adopted from Chanda *et al.*, 2020a).

3.1 Soundscape

The term 'soundscape' has been used by a variety of disciplines to describe the relationship between the landscape (or waterscape) and the relative composition of all sounds present therein (Pijanowski *et al.*, 2011; McWilliam and Hawkins, 2013). In shallow water, the ambient sound field generally consists of various types of sound sources such as biophony, anthrophony as well as the geophony. Here, the analysis of fish sounds (biophonies) and abiotic sounds such as wind and flow sound (geophony) and sounds of the boat (anthrophony) are carried out. The spatial structure of the sound field is dependent on the nature of the waveguide which forms due to the multipath propagation between the sea surface and seabed (Jensen *et al.*, 2011). Therefore, the characteristics of any signal received at a recorder's location can be affected by the variability in environmental parameters. While these propagation features are acknowledged, this research aims to quantify the soundscape and fish acoustic signals as received at the recorders to serve as a representation of what others may receive from their environment in their given locations. The study locations are well-known for tidal-stream influence such as seawater inflow, freshwater runoff, and salinity variations mainly during the southwest monsoon seasons (Manikandan *et al.*, 2016; Sreekanth *et al.*, 2015). Moreover, the variability in the soundscape arises from the bathymetric

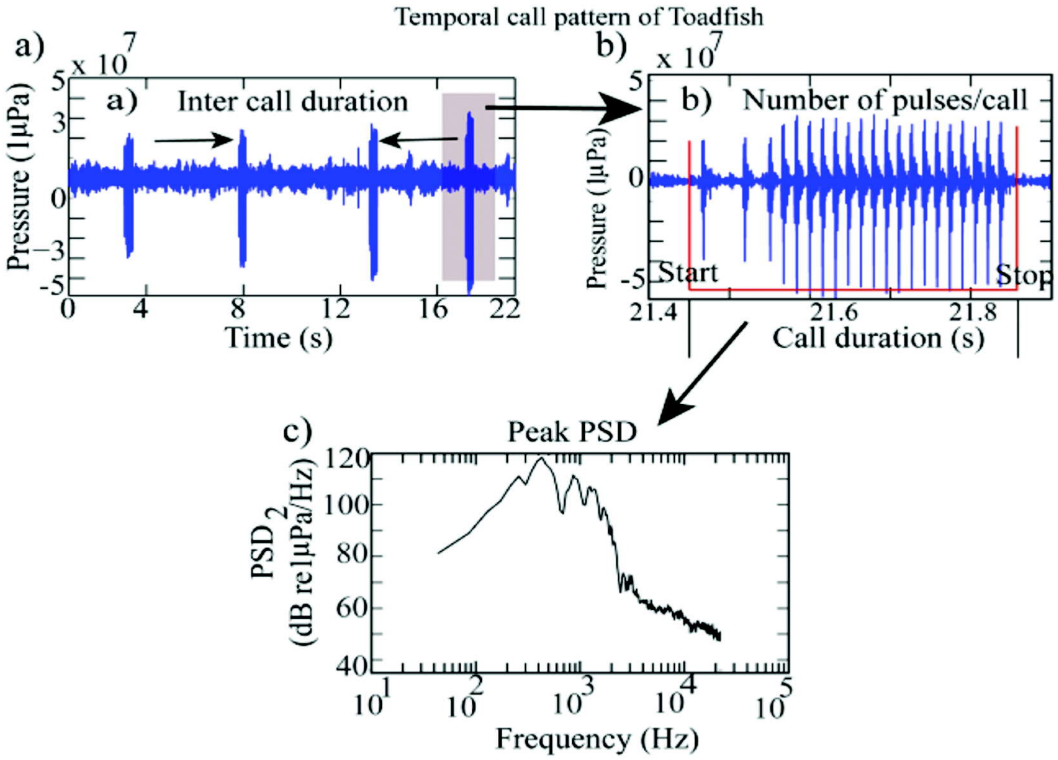

Fig. 3. Temporal and spatial parameters of the fish sound data.

relief, an active shipping channel, frequent small boat transits and biological sounds. The study objectives will include identification of fish species using their vocalizations, and characterization of recorded biophony to understand their relationships using passive acoustic data from ecologically important shallow water regions off Goa. from West Coast of India (WCI).

3.2 *Fish sound characteristics*

The present location is situated towards the deeper end at 30 m water depth, away from the coral reef system near Grande Island. SM2M+ - a passive acoustic data acquisition system was moored midway in the water column. The passive acoustic data acquisition was carried out from 07-12 May 2015 from the present location. The analyses of the concatenated PSD data reveal three types of sounds. Fish sound (indicated as 2 in Fig. 4a), the anthropogenic sound (boat sound indicated as 1), and another kind of sound probably from metal chains used by boats to anchor during the period starting from 07:00 h (on 11 May 2015) to 03:00 h (of 12 May 2015) (indicated as 3). The wind data reveal high-speed winds due to the pre-monsoon session, especially during the period 11-12 May 2015, having an average value of 4.20 m/s [0.5 (min.) to 9.25 (max.) m/s]. The analysis of time series data indicates a daily fish chorus from the early hours of dawn (02:30-06:00 h) (Fig. 4a). The grunting fish sound signatures are symptomatic that are also observed in the data. The waveform, spectrogram, and peak PSD of a single fish call have been depicted (Fig. 4b-d). The PSD of the sound data substantiates the presence of the fish sound (Location 4) near Grande Island. The peak level of the PSD for fish chorus sounds is found to be within the (95.0±2.6 dB re1µPa^2/Hz) (Fig. 4d), and the peak frequency of the PSDs of the fish chorus sounds is noted (289.06±74.93 Hz). We determined temporal parameters of each segmented calls, and average value of the 1726 calls are found to be (call duration: 0.85.0±0.12 sec), (no. of pulses/call: 10.20.0± 1.82 sec), and (inter call duration: 2.36 ± 1.08 sec). The fish sound signals were identified as the grunting sound of the Haemulidae family using the waveforms (Fish and Mowbray, 1970). The temporal call parameters such as call duration, the number of pulses per call, and inter-call duration determined from waveforms along with the spectral peak of

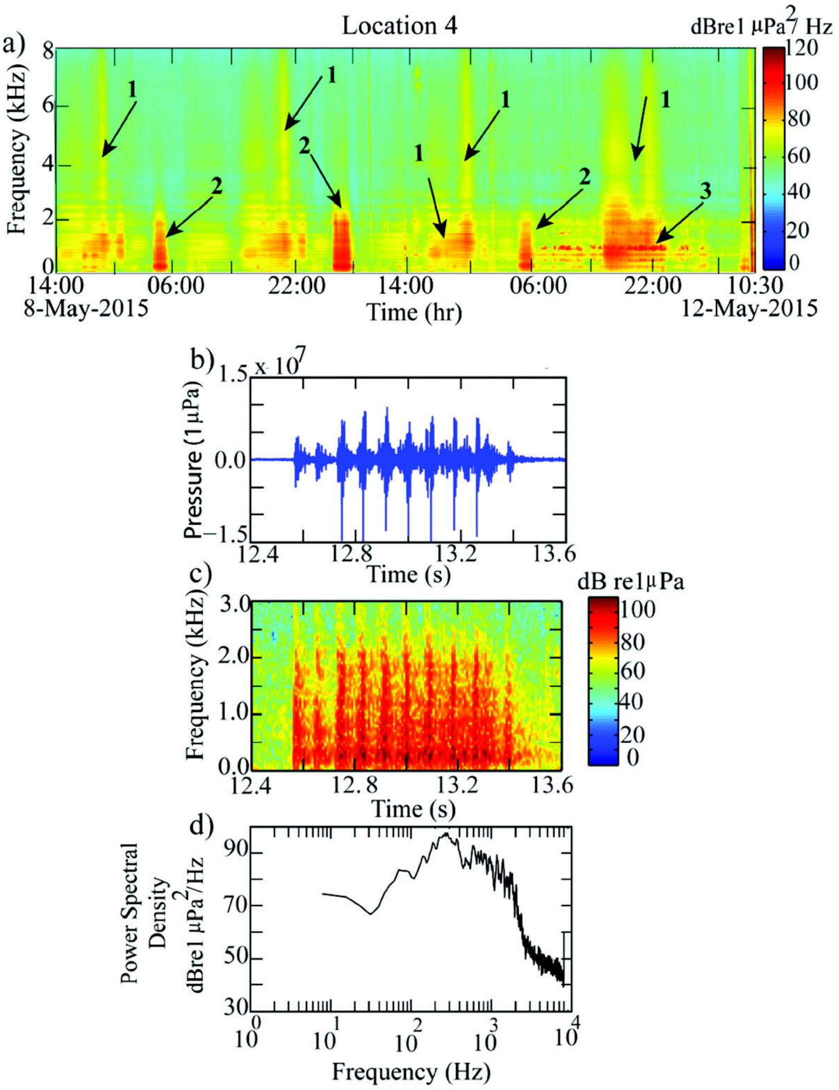

Fig. 4. Concatenated power spectral density (PSD) in dB re 1µPa²/Hz concerning the time in hr at an interval of 15 min, b) waveform (1 µ Pa) versus time (s), c) spectrogram and *c*) Power spectral density in (dB re 1µPa²/Hz) for Haemulidae family of Grunter fish which is similar to Barred Grunt *(Conodon Nobilis)* (given arrows are discussed in the text).

the PSD are also estimated. The single call parameters, including peak frequency, corroborate with the species *Conodon nobilis* (Pombo *et al.*, 2014; Fish and Mowbray, 1970) having a family name: Haemulidae. This fish uses stridulation mechanisms to produce sound (pharyngeal teeth), which is then amplified using a swim bladder (http://www.fishbase.org/). These sounds are associated with feeding. Both males and females produce sounds when the fish is distressed.

Interestingly four fish species of Haemulidae families are reported within the Zuari estuary (close to Grande Island). They are: *Plectorhincus Chubi, Plectorhincus gibbosus, Pomadasys guoraca,* and *Pomadasys furcatus* (Sreekanth *et al.,* 2018). No records of their sounds are available to date. Here we have recorded the sound, which is very much similar to the *Condon nobilis* (also known as a Barred grunt) of Haemulidae families from Caraguatatuba Bight from southeastern Brazil (Pombo *et al.,* 2014) in the Western Atlantic Ocean (fishbase.org). Fish and Mowbray (1970) have provided vocalization details for grunter sound acquired from many parts of the world including *condon nobilis* species of Haemulidae family. Unfortunately, such records are unavailable for the Arabian Sea and adjacent coasts. Therefore, we can surmise that sound data characterized and presented from Grande Island belongs to Haemulidae family, however, confirmation of species out of four species needs more research.

4. CONCLUSION

In this work, we highlighted the importance of a passive acoustic survey to record fish vocalization and related identification. Analyses of the soundscape records acquired at 30m water depth are carried out along with the anthropogenic sound. An algorithm to segment the recorded data is described. We identified that the recorded fish sound from Grande Island is similar to the *Condon nobilis* (also known as a Barred grunt) of the Haemulidae family (Fish and Mowbray, 1970). However, such sounds are not stated from this area, though four species of the Haemulidae family is reported using gillnet fishing.

5. ACKNOWLEDGMENTS

The authors gratefully thank for the support by Dr. Sunil Singh Director, and Dr. S.W.A Naqvi (former-Director) CSIR–National Institute of Oceanography, for their encouragement to carry out this work. We thank Dr. Sundar for the current meter and K. Vijay Kumar for the wind data.

6. REFERENCES

[1] Balk, H., 2001. Development of hydroacoustic methods for fish detection in shallow water. *Faculty of Mathematics and Natural Science,* Ph.D. thesis, University of Oslo.

[2] Shabangu F.W., Coetzee J.C., Hampton I., Kerwath S.E., de Wet W.M. and Lezama-Ochoa A., 2014. Hydro-acoustic technology and its application to marine science in South Africa. *Marine and Maritime Sectors.,* p. 122.

[3] Urick R.J., 1983. Principles of Underwater Sound, McGraw-Hill, New York.

[4] Mann D.A., Hawkins A.D. and Jech J.M., 2008. Active and passive acoustics to locate and study fish. *In Fish bioacoustics Springer, New York*, pp. 279-309.

[5] Popper A.N. and Hawkins A. (Eds.), 2012. The effects of noise on aquatic life. *Springer, New York,* **II,** 1292.

[6] Tyack P.L., Frisk G., Boyd I., Urban E. and Seeyave S., 2015. *International Quiet Ocean Experiment science plan.*

[7] Southall B.L., Bowles A.E., Ellison W.T., Finneran J.J., Gentry R.L., Greene JR, C.R., Green D., Kastak D.R., Ketten J.H., Miller P.E., Nachtigall W.L., Richardson W.J., Thomas J.R. and Tyack P.L., 2007. Overview. *Aquatic mammals.,* **33,** 411.

[8] Tavolga W.N., 1971. Sound production and detection. In Fish physiology, pp. 135-205. Ed. by W. S. Hoar, and D.J. Randall. Academic Press, New York.

[9] Ainslie M.A., 2012. Potential causes of increasing low frequency ocean noise levels. *Journal of the Acoustical Society of America.,* **129,** 2497-2497.

[10] Nystuen J.A., Amitai E., Anagnostou E.N. and Anagnostou M.N., 2008. Spatial averaging of oceanic rainfall variability using underwater sound, Ionian Sea rainfall experiment 2004. *The Journal of the Acoustical Society of America.,* **123,** 1952-1962.

[11] Dahl P.H., Miller J.H., Cato D.H. and Andrew R.K., 2007. Underwater ambient noise. *Acoustics Today.,* **3,** 23-33.

[12] Tyack P.L., 2008. Implications for marine mammals of large-scale changes in the marine acoustic environment. *Journal of Mammalogy.,* **89,** 549-558.

[13] Gervaise C., S. Vallez, C. Ioana, Y. Stephan and Y. Simard., 2007. Passive acoustic tomography: New concepts and applications using marine mammals, A review. *Journal of the Marine Biological Association of the United Kingdom,* **87,** 5-10.

[14] Pace N.G. and Jensen F. (Eds.)., 2002. Impact of littoral environmental variability on acoustic predictions and sonar performance. *Springer Science and Business Media.*

[15] Bertucci F., Parmentier E., Lecellier G., Hawkins A.D. and Lecchini D., 2016. Acoustic indices provide information on the status of coral reefs: an example from Moorea Island in the South Pacific. *Scientific reports.,* **6,** 33326.

[16] Pijanowski B.C., Villanueva-Rivera L.J., Dumyahn S.L., Farina A., Krause B.L., Napoletano B.M., Stuart H.G. and Pieretti N., 2011. Soundscape ecology, the science of sound in the landscape. *BioScience.,* **61,** 203-216.

[17] Weilgart L., 2018. The impact of ocean noise pollution on fish and invertebrates. Report for Ocean Care, Switzerland. URL: https://www oceancare.org. /wpcontent/uploads/2017/10/ OceanNoise_FishInvertebrates_May.

[18] Hastings M.C., Popper A.N., Finneran J.J. and Lanford P.J., 1996. Effects of low-frequency underwater sound on hair cells of the inner ear and lateral line of the teleost fish Astronotus ocellatus. *The Journal of the Acoustical Society of America.,* **99,** 1759-1766.

[19] Hawkins A. D. and Popper A.N., 2017. A sound approach to assessing the impact of underwater noise on marine fishes and invertebrates. *ICES Journal of Marine Science.,* **74,** 635-651.

[20] Fine M.L. and Parmentier E., 2015. Mechanisms of fish sound production. *In Sound communication in fishes Springer, Vienna,* pp. 77-126.

[21] Parmentier E. and M.L. Fine, 2016. Fish Sound Production: Insights, (Eidited by), R.A. Suthers, W.T. Fitch, R. R. Fay, and A.N. Popper, Vertebrate Sound Production and Acoustic Communication, *Springer, Cham,* pp. 19-50.

[22] Vasconcelos R.O., Simoes J.M., Almada V.C., Fonseca P.J., Clara M. and Amorim P., 2010. Vocal Behavior During Territorial Intrusions in the LusitanianToadfish: Boatwhistles Also Function as Territorial'Keep-Out' Signals, *Ethology.,* **116,** 155-165.

[23] McWilliam J.M., Hawkins A.D., 2013. A comparison of inshore marine Soundscape, *J. Experimental Marine Biology and Ecology.,* **446,** 166-176, 2013.

[24] Jensen F.B., Kuperman W.A., Porter M.B., Schmidit H., 2011. Computational Ocean Acoustics 2nd Ed., *Springer, New York,* pp. 15-60.

[25] Rountree R.A., Gilmore R.G., Goudey C.A., Hawkins A.D., Luczkovich J.J. and Mann D.A., 2006. Listening to fish, applications of passive acoustics to fisheries science, *Fisheries.,* **31,** 433-446.

[26] Au W.W. and Lammers M.O., 2016. Introduction: Listening in the Ocean". *In Listening in the Ocean, Springer, New York,* pp. 1-19.

[27] Fish M.P. and Mowbray W.H., 1970. Sounds of the western North Atlantic Fishes, A reference file of biological underwater sound, rhode island univ kingston narragansett marine lab *(Johns Hopkins Press. Baltimore MD).*

[28] Erbe C., Verma A., McCauley R.D., Gavrilov A., Parnum I., 2015. The marine soundscape of the Perth Canyon, *Progress in Oceanography.,* **137,** 38-51.

[29] McCauley R.D. and Cato D.H., 2000. Patterns of fish calling in a near shore environment in a Great Barrier Reef, Phil Trans. *R. Soc. Lond. B.,* **355,** 1289-1293.

[30] Mahanty M.M., Kannan R., Harikrishnan C. and Latha G., 2015. Terapon theraps chorus observed in a shallow water environment in the southeastern Arabian Sea, *Ind. J. Geo-Mar. Sci.,* **44,** 150-155.

[31] Wilden I., Herzel H., Peters G. and Tembrock G., 1998. Subharmonics, biphonation, and deterministic chaos in mammal vocalization. *Bioacoustics.,* **9,** 171-196.

[32] Chakraborty B., Saran A.K., Sinai D., Kuncolienker., Sreepadaa R.A., Haris K. and William Fernandes. A., 2014. Characterization of Yellow Seahorse Hippocampus kuda feeding click sound signals in a laboratory environment: an application of probability density function and power spectral density analyses, *Bioacoustics.,* **23,** 1-14.

[33] Chanda K., Chakraborty B., Mahale V.P., Latha G. and Fernandes W., 2020a. Characterizing 723 three shallow-water locations off Goa, India, using passive acoustic data, *J. Acoust. Soc. Am.,* **148,** 1536-1551.

[34] Chanda K., Chakraborty B., Vardhan Y.V., Gracias D., Mahanty M.M., Latha G., Fernandes W. and Chaubey A.K., 2020b. Passive acoustic metrics to understand shallow water biodiversity off Malvan area in the west coast of India, *Indian J. Geo-Mar. Sci.,* **49,** 527-536, (http://nopr. niscair.res.in/handle/123456789/54663).

[35] Chanda K., Shet S., Chakraborty B., Saran A.K., Fernandes W. and Latha, G., 2020c. Fish sound characterization using multifractal detrended fluctuation analysis, *Fluctu. Noise Letters,* **19,** 2050008. (https://doi.org/10.1142/S021947752050008X).

[36] Padovese L.R., Martin N. and Millioz F., 2009. Time-frequency and time-scale analysis of Barkhausen noise signals. Proceedings of the Institution of Mechanical Engineers, Part G: *Journal of aerospace engineering.,* **223,** 577-588.

[37] Zimmer W.M., 2011. Passive acoustic monitoring of cetaceans. Cambridge University Press.

[38] Haris K., Chakraborty B., Menezes A., Sreepada R.A. and Fernandes W.A., 2014. Multifractal detrended fluctuation analysis to characterize phase couplings in seahorse *(Hippocampus kuda)* feeding clicks. *The Journal of the Acoustical Society of America.,* **136,** 1972-1981.

[39] Manikandan B., Ravindran J., Mohan H., Periasamy R., Murali R.M. and Ingole B.S., 2016. Community structure and coral health status across the depth gradients of Grande Island, Central west coast of India. *Regional Studies in Marine Science.,* **7,** 150-158.

[40] Sreekanth G.B., Manju Lekshmi N. and Singh N.P., 2015. Fisheries profile of Zuari estuary. *International J. Fish. Aquat. Stud.,* **3,** 24-34.

[41] Pombo M., Denadai M.R., Bessa E., Santos F.B., de Faria V.H. and Turra A., 2014. The barred grunt Conodon nobilis (Perciformes: Haemulidae) in shallow areas of a tropical bight: spatial and temporal distribution, body growth and diet. *Helgoland marine research.,* **68,** 271.

[42] Sreekanth G.B., Chakraborty S.K., Jaiswar A.K. and Zacharia P.U., 2018. An inventory on the coastal finfish and shellfish species of Zuari estuary southwest coast of India, *Indian J. Geo-Mar. Sci.,* **47,** 945-958, (http://nopr.niscair.res.in/handle/123456789/44429).

The Journal of Acoustical Society of India : Vol. 49, No. 1-2, 2022 (pp. 12-20)

Density ratio for inner and outer regions of a Mridangam head

Nishanth P.[1] and Udayanandan K.M.[2]

[1]*School of Pure and Applied Physics, Kannur University, Kerala-670 327, India*

[2]*Nehru Arts and Science College, Kanhangad, Kasaragod-671 315, Kerala, India*

e-mail: udayanandan@gmail.com

[Received: 20-10-2021; Accepted: 20-12-2021]

ABSTRACT

Some of the drums in India are made musical by changing a homogeneous membrane to a heterogeneous one. In this paper we obtain the best density ratio required for the outer and inner membranes to produce harmonics in a Mridangam.

1. INTRODUCTION

Ancient people experienced rhythm from their heartbeat, the sound of rain falling on leaves and the flow of water in the river. The pits on the ground covered with a bark could have been the oldest form of drums. One of the oldest drums mentioned in Vedas was the Bhumi dhundhubhi which consists of a pit on the ground covered with an ox skin[1]. The instruments that consists of a pot covered with animal skin, such as Bheri, are common in ancient times[2]. As the time passed, the drums were constructed with hollow barrels of wood covered with animal skin on both sides[3]. Dhol and Mridanga are the most important among them and their variants are common in different parts of India. Dhol type drums are largely used in festivals and ceremonies. Pakhawaj, Khol in North India, Maddalam in Kerala are drums identical in many aspects with Mridangam. Big drums were difficult to be carried over for long distances and hence small hour glass type drums were created, such as Udukku, Damaru and many other varieties can seen in different places of India. The tuning of drums was not easy, since moisture, temperature etc. affect the pitch but the introduction of multiple layers of animal skin helped to tune the drums to the desired pitch. The drums were not only used for music production but were also used for communication, rituals, and wars[4]. In Natya sastra, drums were classified according to their position used to play, shape and structure. B.C. Deva gives a diverse and systematic classification of drums[5]. Accordingly there are three categories of drums namely struck, rub and pluck types. A representation of the classification is given in Fig. 1.

Plucked drums are not practically seen. Indian drums like Mridangam and Maddalam come under the vessel type with bi-facial and cylindrical features. Tabla is a twin drum under mono facial type. All these drums have a loaded drum head. The stretching because of the loading, helped them to produce musical tones. It is because of this special character we classify them separately under pitched drums. In this paper, we study the characteristics of the pitched drum Mridangam in detail.

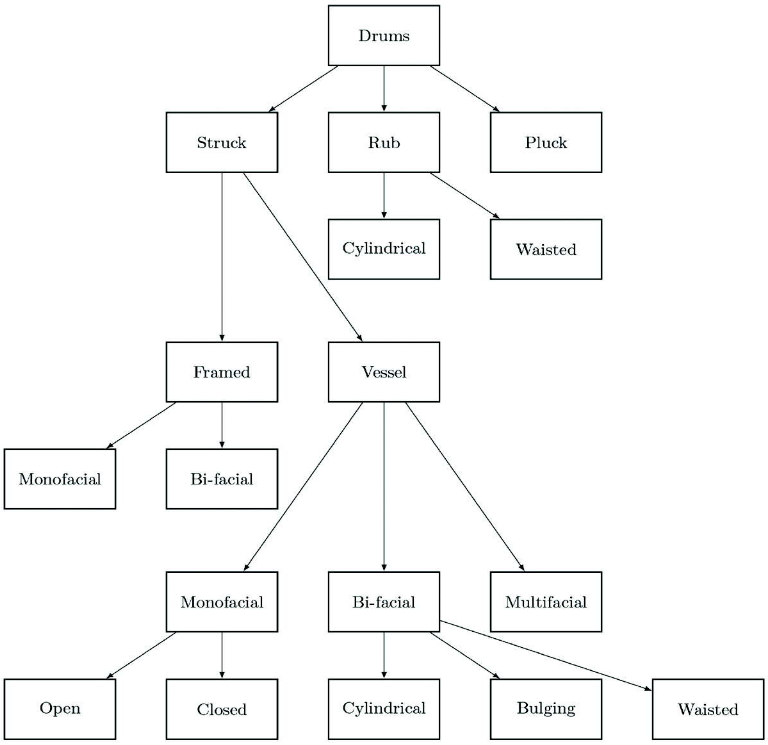

Fig. 1. Classification of Indian drums

2. THE CONSTRUCTION OF THE DRUM HEAD

One or more layers of some animal skin is commonly used to make ordinary drums with a drum head of particular thickness and they produce sound without discriminate pitch. In India, traditionally many homogeneous drum heads are converted to non homogeneous drum heads by fixing a fine paste on the drum head that make their pitch definite. Mridangam, Tabla and Maddalam are some among the drums that possess this special non homogeneous membrane. In Mridangam, there are two heads-left and right. The left head does not have a permanent paste added to the head and it does not produce pitched tones. The right head produces pitched tones. To make the right drum head, 3 layers of goat skin are sandwitched between layers of cow skin. A circular portion at the centre of the topmost layer is removed and a mixture made with Puranakeedam stone powder, rice and glue is pasted several times. The process takes about 2-3 hour. A pasted head of Mridangam is shown in Fig. 2.

Fig. 2. A Mridangam head

3. MODES OF MRIDANGAM

Mridangam produces five pitched sounds. To tune the drum, the stroke Num is used. The frequencies present in Nam stroke of Mridangam tuned to *d* sharp pitch in third octave are shown in Fig. 3. The obtained frequencies and their ratios are given in Table 1.

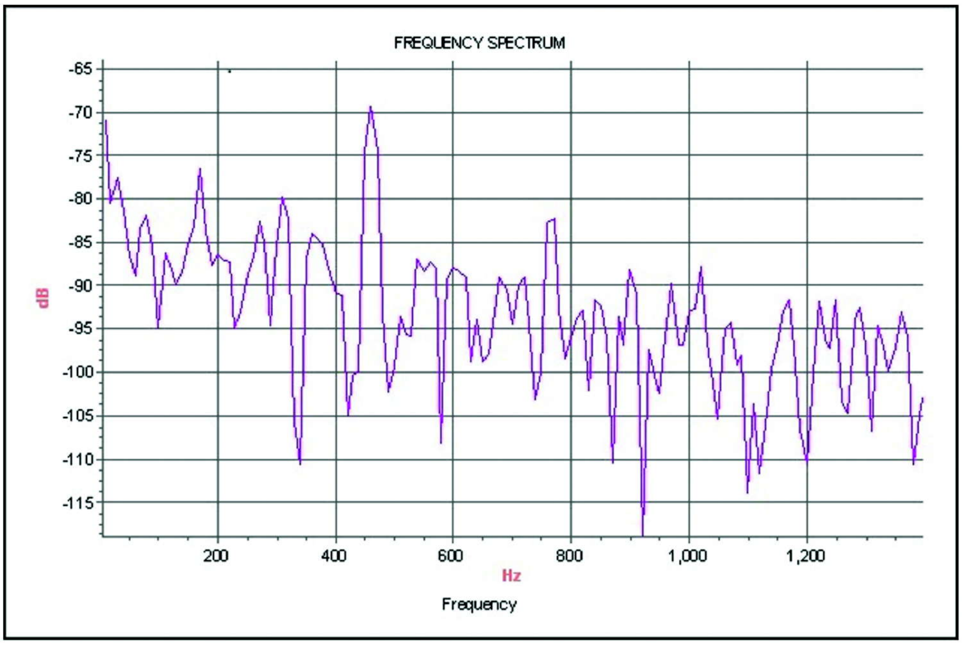

Fig. 3. Frequencies in Mridangam

Table 1. Frequency ratios of the stroke of Mridangam.

Peak	Frequency (Hz)	Ratio
1	168.935	1.09
2	309.148	2.00
3	459.03	2.96
4	599.242	3.87
5	770.881	4.98

4. MODES OF MRIDANGAM

[1]Outside the circular region, along its boundary, there exists an annular region made of animal skin. Hence a Mridangam drum head can be divided into an inner region and an outer region that makes the drum head heterogeneous. Raman[6], Ghosh[7] and Rao[8] studied the vibration of the heterogeneous membrane by choosing power-law variation for mass density. But the modes and their ratio experimentally obtained doesn't match with the power-law variations in density proposed by Raman, Ghosh and Rao. We will give a brief description of the three earlier works in the following subsections.

4.1 Studies by ghosh

For a circular membrane, the wave equation is given by

$$\frac{\partial^2\psi}{\partial r^2}+\frac{1}{r}\frac{\partial\psi}{\partial\psi}+\frac{1}{r^2}\frac{\partial^2\psi}{\partial\theta^2}=\frac{T\partial^2\psi}{\rho\partial t^2} \tag{1}$$

1 Some parts of the studies in this were presented at the 3^{rd} *National Conference on Frontiers in Modern Physics (NCFMP2021)* held at Adamas University, Kolkata on 26-27 November 2021, *Emerging Trends in Physical Sciences (ETPS-2021)* held at ICFAI University, Tripura on 27 September - 01 October 2021 and 26^{th} *International Symposium Frontiers of Research in speech and Music (FRSM-2021)* on 11-12 February 2022 held at IIIT, Pune, Maharashtra.

Let Ψ = *coskt z(r) cosn*θ and $c = \sqrt{\frac{T}{\rho o}}$. Here Ψ is the transverse displacement, k is the wave number, c is the velocity of sound through membrane, t is the time, $z(r)$ is the radial component of transverse displacement, n is an integer and θ is the angular component of transverse displacement. Let the mass density be $\rho = \frac{\rho_o}{r}$ and by using $s = 2k\sqrt{r}$ Eq. (1) changes to

$$\frac{\partial^2 z}{\partial s^2} + \frac{1}{s}\frac{\partial z}{\partial s} + \left(1 - \frac{4n^2}{s^2}\right) z = 0 \tag{2}$$

This is a modified form of Bessel equation and its solution is

$$z = AJ_{2n}(s) \ + \ BY_{2n}(s)$$

At the centre the second part of the above equation does not give a finite solution and hence

$$z = AJ_{2n}(s)$$

$$z = AJ_{2n}(2k\sqrt{r})$$

At the boundary r = a and the vibration is zero. Hence the solution is

$$J_{2n}(2k\sqrt{r}) = 0 \tag{3}$$

From the roots of Eq. (3), the frequency ratios are found. The obtained values are shown in the Table 2. The roots does not form harmonics.

4.2 *Raman's studies*

Raman[9] and Rao[8] also studied density variation in a circular membrane. A power-law variation in the mass density as a function of radius was used by them. The mass density decreases from the centre to the outer edge of the black loaded region. Raman substituted the complete solution of the form

$$\psi = R(r)\cos n\theta \cos(pt - \varepsilon)$$

where n, p are integers and ε is the phase in the wave equation given in Eq. (1) and obtained

$$\frac{d^2R(r)}{dr^2} \ + \ \frac{1}{r}\frac{dR(r)}{dr} \ + \left[\frac{p^2\rho}{T} - \frac{n^2}{r^2}\right]R(r) = 10 \tag{4}$$

Raman used the mass density of the form $\rho = r^{2m-2}$ and using $\frac{p^2}{T} = \lambda^2$ Eq. (4) was modified as

$$\frac{d^2R(r)}{dr^2} + \frac{1}{r}\frac{dR(r)}{dr} + \left[\lambda^2 r^{2m-2} - \frac{n^2}{r^2}\right]R(r) = 0 \tag{5}$$

The solution of Eq. (5) is

$$R(r) = AJ_{\frac{n}{m}}\left(\frac{\lambda}{m}r^m\right) + BY_{\frac{n}{m}}\left(\frac{\lambda}{m}r^m\right) \tag{6}$$

On applying the boundary conditions Eq. (6) changes to

$$J_{\frac{n}{m}}\left(\frac{\lambda}{m}r^m\right) = 0 \tag{7}$$

When m = 1, Eq. (7) is modified at the boundary as

$$J_n(ka) = 0 \tag{8}$$

This is the equation for an ordinary membrane and its roots does not follow the integer ratio.

When $m = \frac{1}{2}$, Eq. (7) is modified at the boundary as

$$J_{2n}\left(2\lambda\sqrt{a}\right) = 0 \tag{9}$$

For Eq. (9), the frequency ratio of various modes are same as for Eq. (3) given in Table 2. The roots

Table 2. Frequency ratios of modes of vibration.

Mode	Frequency ratio
(0,1)	1.0000
(1,1)	2.1355
(0,2)	2.2954
(2,1)	3.1554
(1,2)	3.5001
(0,3)	3.5984

do not produce the observed integer ratio for frequencies of vibration on a heterogeneous membrane.

4.3 Studies by K.N. Rao

In his paper communicated through C. V. Raman, K. N. Rao used mass density of the form

$$\rho = r^{-\gamma}$$

where $\gamma = 2 - 2m$ and substituting this mass density in Eq. (4) and using $\frac{p^2}{T} = \lambda^2$, a differential equation was obtained as

$$\frac{d^2R(r)}{dr^2} + \frac{1}{r}\frac{dR(r)}{dr} + \left[\lambda^2 r^{-(2-2m)} - \frac{n^2}{r^2}\right]R(r) = 0 \tag{10}$$

Eq. (10) has same the solution given by Eq. (6). The second part of the solution becomes infinite at centre and hence the second term from the solution is neglected. So

$$J_{\frac{n}{m}}\left(\frac{\lambda}{m}r^m\right) = R(r) \tag{11}$$

At the boundary, the membrane is fixed at *R(r)* = *a*. Then

$$J_{\frac{n}{m}}\left(\frac{\lambda}{m}a^m\right) = 0 \tag{12}$$

To study the consequences of loading on the drum head, K. N. Rao assumed the density at the boundary to be a constant. To produce a valid finite solution at the origin, the power γ in the density function must be less than zero. To achieve this, m must take values between 0 and 1. For a normalised membrane R = a = 1. When m = 1, $\rho = r^{2\times 1-2} = 1$ and this is the mass density for ordinary membrane. For m = 0 the density $\rho = r^{2\times 0-2} = r^{-2}$.

For the symmetrical vibrations, n = 0 as there is no angular dependence for the vibration. Hence Eq. (12) is modified as

$$J_0\left(\frac{\lambda}{m}\right) = 0 \tag{13}$$

When m = 1, Eq. (13) represents, the eigen value equation of an ordinary circular membrane. When m = 0, the density function goes infinity at the centre of the membrane and the value m = 0 is excluded.

Table 3. Frequency ratio for different m values.

m	First root	Second root	Ratio
0.2	0.480965	1.10402	2.2954
0.4	0.96193	2.20803	2.2954
0.6	1.44287	3.1198	2.2954

Hence m can take values between one and zero. The frequency ratio of (0, 2) mode with different values of m between 1 and 0 are given in Table 3. It is seen that the frequency ratio remains the same with different m.

5. BI-DENSITY MEMBRANE-THEORY

The composite membrane model[10] with two regions of different densities can produce an integer ratio for frequencies of all the modes for Tabla. We are going to find at what density ratio this will happen for Mridangam. In the composite membrane model, the drum head is divided into an inner region and an outer region with radii p, q and mass densities d_1 and d_2 as shown in Fig. 4.

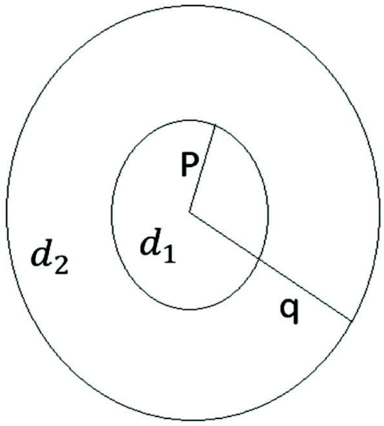

Fig. 4. The representation of two regions on the drum head

Then, $D = \frac{d_1}{d_2}$, the ratio of mass densities and $R = \frac{p}{q}$, the ratio of radii of inner and outer regions on the drum head. For inner and outer regions, the wave equations are

$$\frac{\partial^2\psi_1}{\partial r^2} + \frac{1}{r}\frac{\partial\psi_1}{\partial r} + \frac{1}{r^2}\frac{\partial^2\psi_1}{\partial\theta^2} = \frac{1}{c_1^2}\frac{\partial^2\psi_2}{\partial t^2} \tag{14}$$

$$\frac{\partial^2\psi_2}{\partial r^2} + \frac{1}{r}\frac{\partial\psi_2}{\partial r} + \frac{1}{r^2}\frac{\partial^2\psi_2}{\partial\theta^2} = \frac{1}{c_2^2}\frac{\partial^2\psi_2}{\partial t^2} \tag{15}$$

where $c_1 = \sqrt{\frac{T}{d_1}}$, $c_2 = \sqrt{\frac{T}{d_2}}$. At boundary $\psi_2(q) = 0$. At the circumference of the inner region, the function is continuous, since the entire membrane vibrates when the drum head is struck. To have a finite solution everywhere on the drum head, the function must be differentiable everywhere. Then, the derivative of the function must exist on the entire membrane. Hence

$$\psi_1(p) = \psi_2(p)$$
$$\frac{d\psi_1(p)}{dr} = \frac{d\psi_2(p)}{dr}$$

These are the conditions used to solve the wave equations of two regions. Using these conditions Ramakrishna and Sonthi arrived at an eigen value equation that give integer ratio for frequencies of different modes. The model also produced the frequency ratio of degenerate modes observed in Tabla sound. The ratio of frequencies of modes are found from eigen value equation given by

$$D\frac{J_{n-1}(DRx)}{J_n(DRx)} = \frac{Y_n(x)J_{n-1}(Rx) - J_n(x)Y_{n-1}(Rx)}{Y_n(x)J_n(Rx) - J_n(x)Y_n(Rx)} \tag{16}$$

where $J_n(Rx)$ is Bessel function of first order and $Y_n(Rx)$ is the modified Bessel function of first order.

6. OBSERVATIONS

A commonly played Mridangam also have a pasted inner region and an outer region like Tabla. A practical Mridangam has a radius of 4 cm for its pasted region and it has 9 cm radius for its outer region on the drum head. Hence our R is 0.44. Using the mass density ratio D = 3.125 suggested in reference[10] we get frequency ratios as given in Table 4. The ratios showed much deviation from expected integer values.

In reference[10] Ramakrishna and Sonthi identified R = 0.4 in commonly used Tabla. By keeping R = 0.4, different values of D are given to obtain the frequency ratio of different modes. The frequency ratio of modes of vibration calculated by fixing R and choosing different values of D in Eq. (16) are given in

Table 4. Frequency ratios for R = 0.44 and D = 3.125

Mode	Frequency ratio
(0,1)	0.95
(1,1)	1.81
(0,2)	2.85
(2,1)	2.72
(1,2)	3.84
(3,1)	3.64
(0,3)	4.73
(2,2)	4.84
(4,1)	4.54

Table 5. The frequency ratio of the lowest mode is obtained around 1 at D = 3. An increment of 0.1 for the value of D made the value closer to one. A further increment of 0.05 is made to D and the ratio of lowest mode turned out as less than 1. Hence for further calculation, the mean value between 3.1 and 3.15 is chosen and frequency ratios are found. The process is repeated and an appropriate ratio is obtained at D = 3.140625. By choosing the different values of D it is seen that as the mass density ratio increases, the frequency ratio decreases. Frequency ratio with good harmonic relationship is obtained at D = 3.140625. The instrument makers produce a black pasted region on the drum head in such a way that radius ratio and mass density ratio is achieved in this range.

Table 5. Frequency ratios of modes.

Mode	Frequency ratio for R = 0.4						
	D=3	D=3.1	D=3.125	D=3.1375	D=3.140625	D=3.14375	D=3.15
(0,1)	1.04	1.01	1.00	1.00	1.00	1.00	0.99
(1,1)	2.02	1.96	1.94	1.94	1.94	1.93	1.93
(0,2)	3.17	3.09	3.07	3.06	3.05	3.05	3.05
(2,1)	3.07	2.98	2.96	2.95	2.95	2.95	2.94
(1,2)	4.24	4.14	4.12	4.11	4.10	4.10	4.09
(3,1)	4.14	4.02	3.99	3.97	3.97	3.97	3.96
(0,3)	4.93	4.86	4.85	4.84	4.84	4.83	4.83
(2,2)	5.30	5.20	5.17	5.16	5.16	5.15	5.15
(4,1)	5.19	5.03	4.99	4.97	4.97	4.96	4.96

According to Raman, five sustained musical tones are produced by Mridangam. From Table 5 it is seen that fundamental mode (0, 1) and first overtone mode (1, 1) have independent frequency ratios. Modes (0, 2), (2, 1) have ratios around 3.00. They vibrate with nearby frequency and they are degenerate modes. Hence the vibrations of these modes create a single harmonic tone. Similar ratios are seen for (1, 2) and (3, 1) modes and they are also degenerate modes of vibration. So, single tone is produced by (1, 2) and (3, 1) modes. The vibration of three modes (0, 3), (2, 2) and (4, 1) produce ratios around 5.00 and they also forms a set of degenerate modes that produce a single tone. Hence all the tones identified by Raman in his experiment are found from the model.

The drum Mridangam originated in ancient times and hence its construction must have changed many times with many modifications. The word Mridangam itself indicates part made with mud and the descriptions in literature like Natyasastra shows that the central loaded region on the drum head was earlier made with mud[11-12]. Subsequently, loading with stone and rice emerged and is now common in use.

As the construction evolved with time, mostly trial and error methods, no standardisation in the parameters or process can be seen. Hence the exact value of either mass density ratio or radius ratio is not followed by the makers. In 2006, S. Gaudet *et al.* mathematically tried to answer the possibility of other configurations for Tabla[13]. They found new configuration of Tabla at D = 2.9 and k = 0.38. We calculated the frequency ratios of Tabla with the values given by Gaudet et al. and the obtained ratios are tabulated in Table 6. In this new configuration unlike one predicted by Ramakrishna and Sonthi, the fifth harmonic tone is produced by modes (1, 3), (2, 2) and (4, 1). The ratio of (0, 3) is shifted near to 6.00 which indicates that the mode contributes a new tone. Hence in this new configuration, Tabla can generate 6 harmonic tones.

Table 6. Frequency ratios for R = 0.38 and D = 2.9

Mode	Frequency ratio
(0,1)	1.00
(1,1)	1.95
(0,2)	3.05
(2,1)	2.99
(1,2)	4.02
(3,1)	4.05
(0,3)	5.98
(1,3)	5.13
(2,2)	4.95
(4,1)	5.09

Table 7. Frequency ratios of modes.

Mode	Frequency ratio for R = 0.38						
	D=2.5	D=2.75	D2.8125	D=2.84375	D=2.8515625	D=2.859375	D=2.875
(0,1)	1.00	1.00	1.00	1.00	1.00	1.00	1.00
(1,1)	1.94	1.95	1.95	1.95	1.95	1.95	1.95
(0,2)	2.95	3.02	3.03	3.04	3.04	3.04	3.04
(2,1)	2.96	2.98	2.99	2.99	2.99	2.99	2.99
(1,2)	3.76	3.93	3.97	3.99	3.99	3.99	4.00
(3,1)	4.02	4.04	4.05	4.05	4.05	4.05	4.05
(0,3)	4.21	5.95	5.96	5.97	5.97	5.97	5.98
(1,3)	4.92	5.04	5.08	5.10	5.10	5.11	5.12
(2,2)	4.52	4.79	4.86	4.89	4.90	4.91	4.92
(4,1)	5.07	5.09	5.09	5.09	5.09	5.09	5.09

By keeping R = 0.38 we analysed the possible values of D for Mridangam. Using Eq. (16) the obtained values are given in Table 7. Good harmonic relationship for frequency ratio is obtained at D = 2.8515625 by keeping the maximum deviation from integer ratio as 0.1.

A further improved frequency ratios are obtained by changing R to 0.384 at D = 2.835. The obtained ratios are shown in Table 8. The obtained value of R indicates that the pasted region span across 38.4 percent of the radius of the drum head in Mridangam.

Table 8. Frequency ratios for R = 0.384 and D = 2.835

Mode	Frequency ratio
(0,1)	1.00
(1,1)	1.95
(0,2)	3.03
(2,1)	2.98
(1,2)	3.99
(3,1)	4.03
(0,3)	5.96
(1,3)	5.10
(2,2)	4.90
(4,1)	5.06

7. CONCLUSIONS

In Mridangam, the mass density and radii of two regions on the membrane influences the ratios produced by the drum. In South Indian music two variants of Mridangam are commonly played - male and female. Male Mridangam is a low pitched Mridangam whereas female Mridangam is played at high pitch. Generally, pitch and the radius of Mridangam are inversely related. Hence the first configuration with R = 0.4 and D = 3.140625 represents a male variant. The second configuration with R = 0.384 and D = 2.835 represent a female type.

ACKNOWLEDGEMENTS

The author Nishanth P. acknowledge the help of Mr. Arjun P.P. for giving the Mridangam sound samples for the studies done.

REFERENCES

[1] Ranade A.D., 2005. Drums of India: an ethnomusicological perspective, Sangeet Natak J. Sangeet Natak Akad. *JSNA,* **39**(2), 47-57.

[2] Dean M., 2011. The Drum, A History, Scarecrow Press.

[3] Krishnaswami S., 2017. Musical Instruments of India, Publications Division Ministry of Information & Broadcasting, India.

[4] Shakuntala K.V., 1968. Martial Musical Instruments of Ancient India, Sangeet Natak J. Sangeet Natak Akad. *JSNA,* **10,** 5-11.

[5] Deva B.C., 1978. Musical Instruments of India, Their History and Development, Calcutta, Firma KLM.

[6] Raman C.V. and Sivaraj Ramaseshan, 1988. Scientific Papers of C.V. Raman, *Indian Academy of Sciences,* **2**.

[7] Ghosh R.N., 1922. Note on Musical Drums, *Phys. Rev.,* **20**(6), 526-527.

[8] Rao K.N., 1938. Theory of the Indian Musical Drums-Part I, *Proc. Indian Acad. Sci.-Sect. A,* **7**(2), 75-84.

[9] Raman C.V., 1927. Musical instruments and their tones, *Handbuch Der Physik, Chapter,* **8,** 354-424.

[10] Ramakrishna B.S. and Sondhi M.M., 1954. Vibrations of Indian Musical Drums Regarded as Composite Membranes, *J. Acoust. Soc. Am.,* **26**(4), 523-529.

[11] Raghavan V., 1953. Why is the Mridanga so -called?, *J. Music Acad. Madras,* **24,** 135-136.

[12] Raghavan V., 1955. Why is the Mridanga so-called?, *J. Music Acad. Madras,* **26,** 148.

[13] Gaudet S., Gauthier C. and Leger S., 2006. The Evolution of Harmonic Indian Musical Drums. A Mathematical Perspective, *J. Sound Vib.* **291**(1-2), 388-394.

The Journal of Acoustical Society of India : Vol. 49, No. 1-2, 2022 (pp. 21-27)

Marine propeler noise control by ducted isolation – A study

V. Rama Krishna[1*], CH. Kishore[2], PVS Ganesh Kumar[1] and C. Naga Raju[2]
[1]*Naval Science and Technological Laboratory, Visakhapatnam, India*
[2]*VR Siddhartha engineering college, Vijayawada, India*
e-mail: ramki40@gmail.com

[Received: 18-01-2021; Accepted: 10-01-2022]

ABSTRACT

The present work aims at a numerical study of controlling the propeller noise by using the method of isolation. In this method four types of ducts are modeled around 6 bladed propellers and are analyzed. Cylindrical, Profile, Convergent and Convergent-divergent ducts are studied. Unsteady non-cavitating noise of ducted propellers at its rotating speed and vehicle speed is predicted. Numerical simulations are carried out using a finite volume code FLUENT. The output of CFD results is used for Acoustic analysis. The methodology adopted in CFD analysis is large eddy simulation (LES) and in acoustical analysis it is Ffowcs William's-Hawkings (FW-H) formulation. Noise spectrum is predicted over the frequency range of 0-2 kHz. From this numerical study on these propellers, duct configuration for least noise and better performance of propeller is identified.

1. INTRODUCTION

Propeller noise mainly depends on Propeller geometry, Propeller wake inflow, and Propeller isolation. Due to the pressure difference in rear and aft end of the propeller blade the noise is generated. Reducing pressure oscillations on the propeller is one of the most effective ways of reducing the radiated noise. The parameters which influence the noise levels produced by the propeller are number of blades, pitch angle, blade area, diameter of blade, skew angle, Trailing edge geometry and Propeller blade finishing fineness. This noise can also be reduced by designing a duct around the propeller and this method is known as propeller isolation. In this study, an existing six bladed propeller is selected. Four types of ducts are designed around the propellers which are cylindrical duct, profile duct, convergent duct and convergent-divergent duct. The prediction of non-cavitation noise of propeller is carried out by using FW-H equation and eddy viscosity model of large eddy simulation (LES) in computational fluid dynamics Fluent software. The study resulted in understanding the effect of ducts on propeller noise.

2. LITERATURE REVIEW

Over the years Propeller noise control has been studied by various researchers. In this section some of the studies reported by researches on topic are presented.

K. P. Santhosh Babu ***et al.*** **(1) :** Marine ducted propeller is a rotating duct fan that is used on tugs and trawlers which creates a greater propulsive thrust force to drive over a water medium in heavy working condition in harbor. This paper progresses with comprehensive information of marine ducted propeller having blade made of aluminum alloy and duct of alloy steel designed and analyzed with various blade formations of 4 and 5 separately. Main aim is to check the performance of each blade individually to show which blade performs better with maximum velocity rate under stream line motion in water at dynamic condition. Ducted propeller is modeled in solid works. Hydrostatic and hydrodynamic analyses of each blade are performed with ANSYS workbench

R. Bontempo *et al.* (2) : This paper depicts the investigation of the flow around a ducted propeller ducted with a so-called accelerating duct. In this paper, axial momentum theory and nonlinear actuator disk methods are used. The straightforward application of the first approach reveals that if the duct and rotor thrusts are concordant, then a beneficial effect on the propulsive efficiency can be readily obtained by enclosing a propeller in an accelerating duct. When the more advanced nonlinear actuator disk method is applied to verify the outcomes of the axial momentum theory additional information on the performance of the device are obtained. Moreover, the non-linear actuator disk method is also employed to investigate, through experimental design techniques, the effect of the key geometrical parameters of the duct on the efficiency and robustness of this kind of propulsive system. In particular, it has been found that a propulsive efficiency gain can be achieved through a duct thickness, camber and chord increase, and through an inci-dence decrease.

Mehdi Chamanara *et al.* (3) : In their study, the effect of the duct angle and propeller location on the hydrodynamic characteristics of the ducted propeller using Reynolds-Averaged Navier Stokes (RANS) method is reported. A Kaplan type propeller is selected with a 19A duct. The ducted propeller is analyzed by three turbulence models including the k-ε standard, k-ω SST and Reynolds stress model (RSM). The numerical results are compared with experimental data. The effects of the duct angle and the location of the propeller inside the propeller are presented and discussed.

Tadeusz Koronowicz *et al.* (4) : This article describes new computer system which is specific for the design of ducted propellers. This system concerns first of all the procedures for the design calculation of ducted propellers and for the analysis of the ducted propeller operation in the nonuniform velocity field behind the ship hull. The comparative analysis of computation results for different types of ducts is also presented.

João Manuel Baltazar *et al.* (5) : In their work, a comparison between the results obtained by a panel code with a Reynolds-averaged Navier-Stokes (RANS) code is made to obtain a better in-sight on the viscous effects of the ducted propeller. They also studied the limitations of the inviscid flow model, especially near bollard pull conditions or low advance ratios, which are important in the design stage. From the comparison, several modeling aspects are studied for improvement of the inviscid (potential) flow solution. Finally, the experimental open-water data is compared with the panel method and RANS solutions. A strong influence of the blade wake pitch, especially near the blade tip, on the ducted propeller force predictions is seen. A reduction of the pitch of the gap strip is proposed for improvement of the performance prediction at low advance ratios.

3. BRIEF DESCRIPTION OF PROPELLER

The dimensions of the reference propeller configuration studied are mentioned in Table 1.

Propeller blade is made of Forged Aluminium Al-24345 alloy and its Material Specifications are depicted in Table 2.

Table 1. Dimensions of Reference propeller model.

Diameter (m)	0.389 m
Expanded Area ratio, EAR = A_E/A_0	0.58
Number of Blades	6
Hub ratio	0.245
Series	NACA 66

Table 2. Material Specifications.

Density (kg/m^3)	2689.8
Young's Modulus (GPa)	68.3
Poisson's Ratio	0.34
Proof Stress (MPa)	385

4. MODELLING OF DUCTS

Modeling of the propeller was carried out using CATIA V5 R20. The model is generated by using propeller geometry of each section of the blade at various radii *i.e.* main geometrical characteristics of propeller geometry of cylinder blade at different sections.

The dimensions of the four types of ducts namely Cylindrical, Profile, Convergent and Convergent-divergents are given in Table 3.

Table 3. Dimensions of ducts.

Duct	Front side outer radius(mm)	Back side outer radius(mm)	Length (mm)	Thickness (mm)
Cylindrical	195.5	195.5	200	12
Profile	195.5	165	200	12
Convergent	230	165	200	12
Convergent-divergent	230	240	200	12

Model of the 6-blade reference propeller is shown in Fig. 1. Solid models of 4 types of ducts are shown from Fig. 2 to 5.

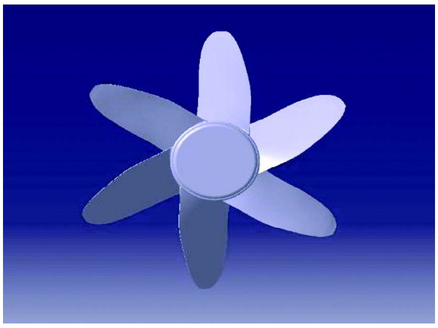

Fig. 1. Reference propeller

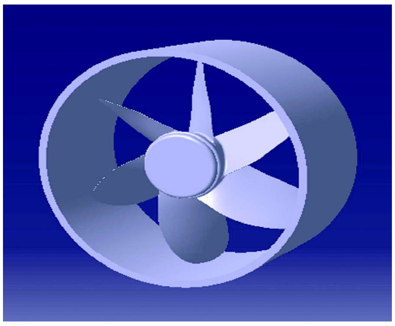

Fig. 2. Cylindrical duct

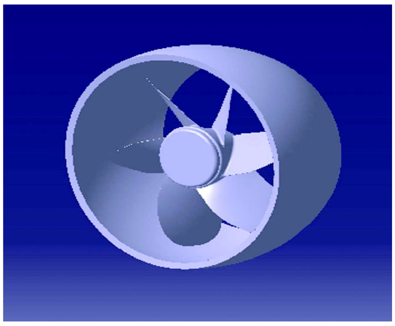

Fig. 3. Profile duct

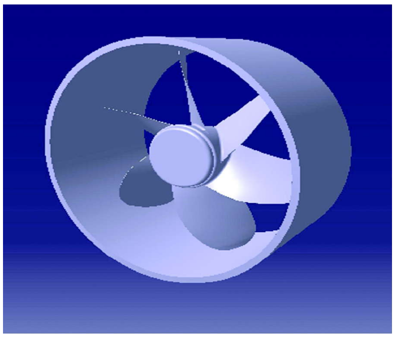

Fig. 4. Convergent duct

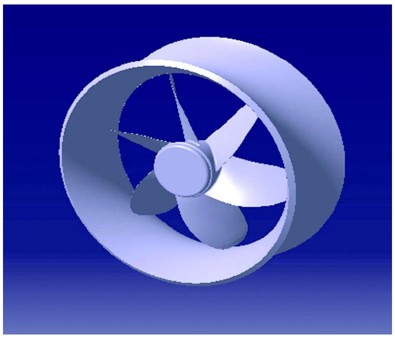

Fig. 5. Convergent-divergent duct

5. ANALYSIS

The modeling approach presented in this paper is similar to the approach by various authors who had contributed their research in the field of propeller duct designs. The aim was to assess the importance of ducts to reduce the induced noise during the operation of propeller. This can lead to a reliable and versatile simulation setup which may be used for tests of different propeller ducts and the selection of best duct with low sound pressure level.

5.1 Meshing

The type of mesh used for this analysis is as follows

Type of Element : Tetrahedral, Mesh type: Fine, Mesh Size: 11 mm.

Number of Nodes and Elements of all 4 types of ducts are as shown in Table 4.

Optimum mesh size of 11 mm is arrived through iterative study by using various mesh sizes.

The meshed model of cylindrical ducted Propeller is shown in Fig. 6.

Table 4. Number of Nodes and Elements of all 4 types of ducts.

S. no	Type of Duct	Number of Nodes	Number of Elements
1	Cylindrical Duct	48306	239855
2	Profile Duct	47154	236178
3	Convergent Duct	47793	243450
4	Convergent-Divergent Duct	45880	234328

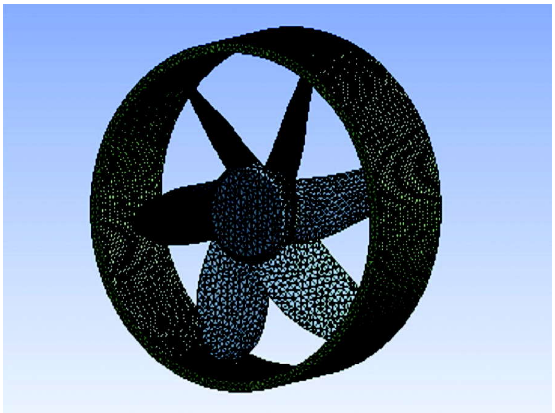

Fig. 6. Meshed model of cylindrical duct

5.2 CFD analysis

Numerical simulations have been carried out with a finite volume module called FLUENT. In the CFD analysis, LES turbulence model is used. Surfaces which can rotate relatively are defined as moving wall and are dependent on the fluid around them. Fluid Zone has to be considered as a cylinder extending either side of the bladed propeller. Cylinder walls are categorized as stationary wall and the inlet and outlet are defined as velocity inlet (7.08 m/sec) and outflow. Fluid zone in the inner volume is defined as moving mesh at 780 rpm in x-direction.

With this configuration, CFD analysis is carried out on all the four kinds of ducted propellers using large eddy simulation (LES).

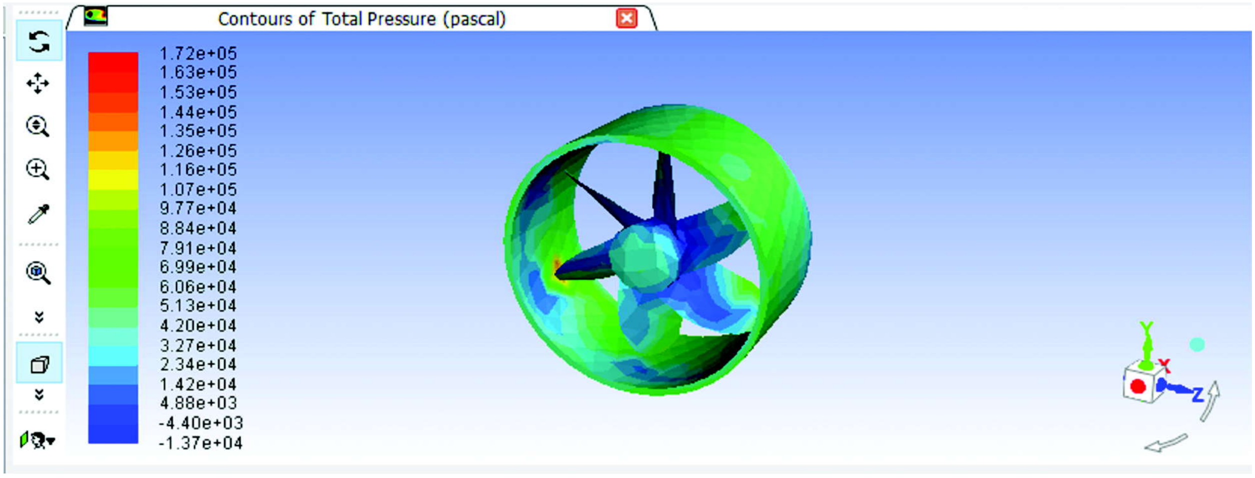

Fig. 7. Total pressure distribution of Cylindrical ducted propeller

Results of CFD analysis of cylindrical ducted propeller is shown in Fig. 7.

6. ACOUSTIC ANALYSIS

The output of CFD results is carried further for Acoustic analysis. Acoustic analysis was done in ANSYS using Ffowcs Williams-Hawkings (FW-H) formulation. Noise spectrum was predicted over the frequency range of 0-2 kHz. Noise spectra for cylindrical ducted propeller is shown in Fig. 8.

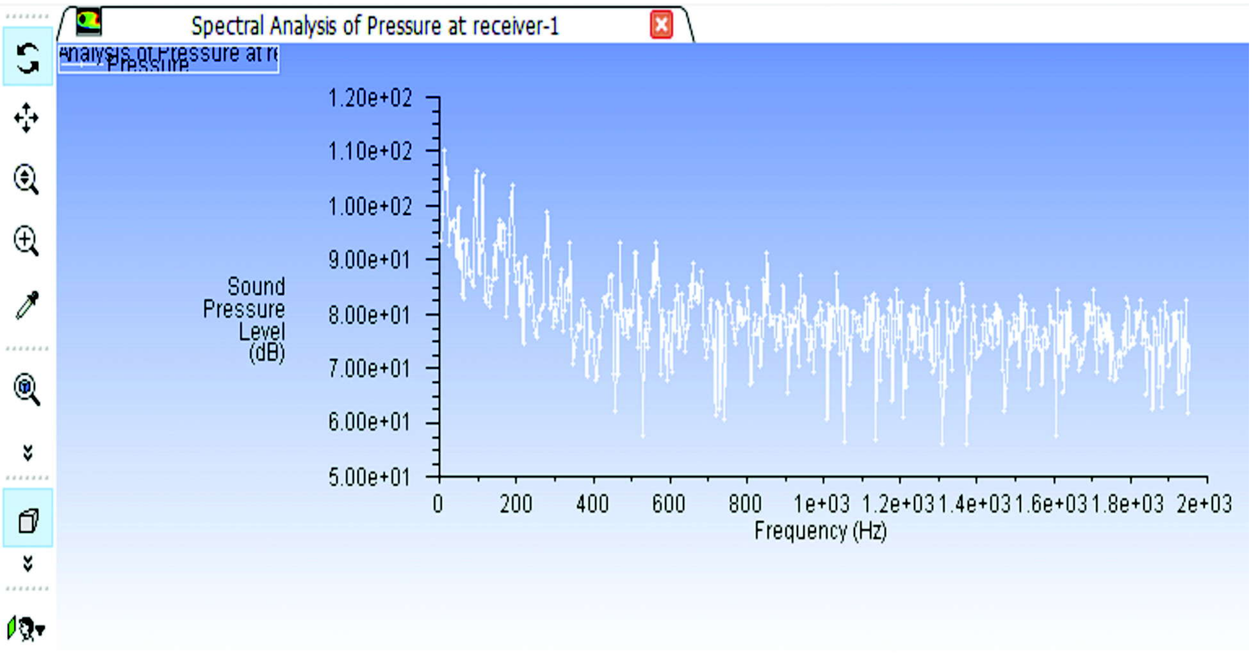

Fig. 8. Frequency vs sound pressure level graph of Cylindrical ducted propeller

6.1 Comparison of Sound pressure level (SPL) of ducted propellers

Sound Pressure level (SPL) of all 6 bladed propeller with four kinds of ducts are given in Table 5.

Table 5. Comparison of SPL of ducted propellers with Reference propeller.

Reference Propeller SPL (dB)	Cylindrical Duct SPL(dB)	Profile Duct SPL(dB)	Convergent Duct SPL (dB)	Convergent divergent Duct SPL (dB)
130	122.5	127	125.6	128

It can be seen from table 5, compared to reference propeller, all ducted propellers provide lesser noise but cylindrical ducted propeller provide least noise among studied configurations.

7. CALCULATION OF THRUST AND TORQUE COEFFICIENTS

Thrust and Torque values of Reference and 04 varieties of ducted Propellers which were obtained from the CFD analysis is shown in Table 6. Operating conditions are :

Density of sea water *(ρ)* =1029 kg/m^3

Diameter of propeller *(D)* =0.389 m

The Thrust and Torque coefficient were calculated from the following equations.

Thrust coefficient, $K_T = \frac{T}{\rho n^2 D^4}$

Torque coefficient, $K_Q = \frac{Q}{\rho n^2 D^5}$

Using the above, Thrust and Torque coefficients are calculated for ducted propeller and reference propeller. A Comparison of Thrust coefficient and Torque coefficients is shown in Table 7.

From the above table, Thrust and Torque coefficients are increased for cylindrical ducted propeller compared to reference propeller. Even though Convergent and Convergent Divergent ducted propellers have higher Thrust coefficient, lower noise is from Cylindrical ducted propeller while satisfying required Thrust and torque.

Table 6. Thrust and Torque of Reference Propeller.

Parameter	Reference Propeller	Cylindrical ducted propeller	Profile ducted propeller	Convergent ducted propeller	Convergent Divergent ducted propeller
Thrust ,T in N	1385.73	1444	1081	5811	2058
Torque, Q in N-m	51.89	74	88	72	73

Table 7. Comparison of Thrust and Torque coefficients of ducted propeller with Reference propeller

Parameter	Reference Propeller	Cylindrical ducted propeller	Profile ducted propeller	Convergent ducted propeller	Convergent Divergent ducted propeller
Thrust coefficient	0.348	0.362	0.271	1.459	0.516
Torque coefficient	0.0335	0.047	0.056	0.046	0.047

7. CONCLUSION

The non-cavitating underwater noise of ducted propellers has been studied through Numerical approaches. It is seen that ducting provides reduction in noise. Further, it is seen that propeller with cylindrical duct generates lesser sound than profile, Convergent-divergent and convergent ducted propeller. Thrust and Torque coefficients are better for cylindrical ducted propeller compared to reference propeller thereby implying that cylindrical ducted propeller is optimum choice.

8. ACKNOWLEDGEMENTS

The authors wish to express their sincere gratitude to Dr.O.R.Nandagopan, outstanding scientist and Director, NSTL Visakhapatnam for permitting to publish this paper.

9. REFERENCES

[1] Santhosh Babu K.P. and Padmanabhan S., 2017. "Design of marine propeller blade with different blade sequences analyze the hydro formation under pressure hydrodynamic fill," *APRN Journal of Engineering and Applied Sciences,* **12,** 17.

[2] Rodolfo Bontempo and Marcello Manna, 2016. "Effects of Duct Cross Section Camber and Thickness on the Performance of Ducted Propulsion Systems for Aeronautical Applications," *International Journal of Aerospace Engineering,* ID 8913901.

[3] Mehdi Chamanara, Hassan Ghassemi, Manouchehr Fadavie and Mohammad Aref Ghas-semi, 2018. "Effects of the duct angle and propeller location on the hydrodynamic characteristics of the ducted propeller," *Ship Science and Technology,* **11**(22), 41-48.

[4] Tadeusz Koronowicz, Zbigniew Krzemianowski, Teresa Tuszkowska and Jan A. Szantyr, 2009. "A complete design of ducted propellersusing the new computer system," *Polish Maritime Research,* **2**(60) **16,** 34-39.

[5] João Manuel Baltazar, DouweRijpkema, José Falcão de Campos and Johan Bosschers, 2018. "Prediction of the Open Water Performance of Ducted Propellers with a Panel Method," *Journal of Marine Science and Engineering,* pp. 6-27.

The Journal of Acoustical Society of India : Vol. 49, No. 1-2, 2022 (pp. 28-35)

Marine propeller noise control using ducts with stator

V. Rama Krishna[1*], P. Srinivasa Rao[2] and Madhu[2]

[1]NSTL, Visakhapatnam, India

[2]AU, Visakhapatnam, India

e-mail: ramki40@gmail.com

[Received: 18-01-2021; Accepted: 10-01-2022]

ABSTRACT

To evade detection by enemies, the underwater-radiated noise of marine vehicles must be reduced. The propeller, machinery, and flow cause this noise. Many researchers devised ways for reducing noise from each of these sources. According to the literature, a reasonable knowledge of machinery noise control has been established, but propeller noise and flow noise management still require further study. Because flow noise contributes so little to underwater radiated noise, propeller noise reduction readily emerges as a worthwhile subject. Propeller noise is controlled in principle by geometry modifications, wake modification and isolation.

The present work aims at a numerical study of controlling the propeller noise by using the method of isolation. In this method, four types of ducts and a stator are modeled around 6 bladed propeller and are analyzed. First type of duct is a cylindrical, second type is profile, third type is convergent duct and fourth type is convergent-divergent duct. Unsteady non-cavitating noise of ducted propellers with stators at its rotating speed and vehicle speed is predicted and studied. Modelling of propellers is carried out using CATIA V5. In order to obtain better results, the numerical simulations are carried out using a finite volume code FLUENT. The methodology adopted in CFD analysis is large eddy simulation (LES) and in acoustical analysis is Ffowcs William's-Hawkings (FW-H) formulation. The output of CFD results is used for Acoustic analysis. Noise spectrum is predicted over the frequency range of 0-2 kHz for 6 bladed propellers of four types of ducts with stator. From this numerical study on these propellers, duct with stator configuration for least noise and better performance of propeller is identified

1. INTRODUCTION

Propeller noise of Marine vehicles like Torpedo, Submarine and Warships is to be controlled from stealth point of view. The radiated noise from the propeller depends on Propeller geometry, Propeller wake inflow, and Propeller isolation. Due to the pressure difference in rear and aft end of the propeller blade the noise is generated. Reducing pressure oscillations on the propeller is one of the most effective ways of reducing the radiated noise. The parameters which influence the noise levels produced by the propeller are changing the number of blades, changing the Pitch angle, change in blade area, changing the diameter of blade, change in Skew angle, Trailing edge geometrical modifications and Propeller blade finishing fineness. This noise can also be reduced by designing a duct around the propeller and this method is known as propeller isolation. In this study, a six bladed propeller of existing propeller is taken as reference, is used and four types of ducts with stator are designed around the propeller which are cylindrical duct with stator, profile duct with stator, convergent duct with stator and convergent-divergent duct with stator. The diameter of propeller is 0.389m and hub to propeller diameter ratio is 0.25. Prediction of non-cavitation noise of propeller was carried out by numerical method at rotating speed of 780 rpm at vehicle speed of 7.08 m/s. The prediction of non-cavitation noise of propeller was done by using FW-H equation and eddy viscosity model of large eddy simulation (LES) in computational fluid dynamics Fluent software. The study resulted in understanding the effect of ducts on decrease and increase of propeller noise.

2. LITERATURE REVIEW

Over the years Propeller noise control has been studied by various researchers. In this section some of the studies reported by researches on topic are presented.

K. P. Santhosh Babu *et al.* (1) : Marine ducted propellers are rotating duct fan that are used on tugs and trawlers which creates a greater propulsive thrust force to drive over a water medium on heavy working condition in harbor. This paper progresses with comprehensive information of marine ducted propeller having blade made of aluminum alloy and duct of alloy steel is designed and analyzed with various blade formations of 4 and 5 separately. Main aim is to check the performances of each blade individually to show which blade performs efficiently better with maximum velocity rate under stream line motion on water at dynamic condition. Ducted propeller is modeled in solid works. Hydrostatic and hydrodynamic analyses of each blade are performed with ANSYS workbench

R. Bontempo *et al.* (2) : This paper depicts the investigation of the flow around a ducted propeller ducted with a so-called accelerating duct.Main aim is, both the axial momentum theory and a nonlinear actuator disk method are used. The straightforward application of the first approach reveals that if the duct and rotor thrusts are concordant, then a beneficial effect on the propulsive efficiency can be readily obtained by enclosing a propeller in an accelerating duct. When the more advanced nonlinear actuator disk method is applied to verify the outcomes of the axial momentum theory additional information on the performance of the device are obtained. Moreover, the nonlinear actuator disk method is also employed to investigate, through experimental design techniques, the effect of the key geometrical parameters of the duct onto the efficiency and robustness of this kind of propulsive system. In particular, it has been found that a propulsive efficiency gain can be achieved through a duct thickness, camber and chord increase, and through an incidence decrease.

Mehdi Chamanara *et al.* (3) : In this study, the effect of the duct angle and propeller location on the hydrodynamic characteristics of the ducted propeller using Reynolds-Averaged Navier Stokes (RANS) method is reported. A Kaplan type propeller is selected with a 19A duct. The ducted propeller is analyzed by three turbulence models including the k-ε standard, k-ω SST and Reynolds stress model (RSM). The numerical results are compared with experimental data. The effects of the duct angle and the location of the propeller inside the propeller are presented and discussed.

Tadeusz Koronowicz *et al.* (4) : The computer system for the completed design of the ducted ship propellers has some common blocks andprocedures. This article describes only these blocks and procedures which are specificfor the design of ducted propellers. These new blocks concern first of all the procedures for the designcalculation of ducted propellers and for the analysis of the ducted propeller operation in the non-uniformvelocity field behind the ship hull. The com-parative analysis of computation results for different types ofducts is also presented.

João Manuel Baltazar *et al.* (5) : Inthis work, a comparison between the results obtained by a panel code with a Reynolds-averaged Navier-Stokes (RANS) code is made to obtain a better in-sight on the viscous effects of the ducted propeller. In this paper also studied on the limitations of the inviscid flow model, especially nearbollard pull conditions or low advance ratios, which are important in the design stage. The analysis is carried out for propeller Ka470 operating inside duct 19A. From the comparison, several modeling aspects are studied for improvement of the inviscid (potential) flow solution. Finally, the experimental open water data is compared with the panel method and RANS solutions. A strong influence of the blade wake pitch, especially near the blade tip, on the ducted propeller force predictions is seen. A reduction of the pitch of the gap strip is proposed for improvement of the performance prediction at low advance ratios.

Negin Donyavizadeh (6) : In this study, hydrodynamic performance of the linear jet propulsion system is numerically investigated. Accordingly, the Ansys CFX software is utilized and RANS equations are solved using the SST turbulent model. The results of the proposed numerical model, in the form of thrust and torque coefficient as well as efficiency, are compared with available experimental data for a ducted propeller, and good compliance is achieved. Considering the importance of stator cross section on the performance of the linear jet propulsion system, the influence of thickness and camber size of the stator on linear jet propulsion systems are examined. Based on the numerical findings, it is determined that at constant advance ratio, with increasing thickness of stator, the efficiency increases. It is also observed that as the span length increases, the maximum and minimum of the pressure coefficient increase for different thicknesses. Furthermore, it is seen that positive and negative pressure coefficients decrease with an increase in foil thickness.

3. NUMERICAL MODEL OF PROPELLER

3.1 Modelling of ducts

Modeling of propeller was carried out using CATIA V5 R20. Propeller modeling is carried out by using propeller geometry of each section of the blade at various radii i.e. main geometrical characteristics of propeller geometry of cylinder blade at different sections were used. In this paper four kinds of ducts with stators are modeled around the 6 blade reference propeller is as shown in fig. 1. Solid model of 4 types of ducts with 7 blade stator are shown in below fig. 2 to fig. 6. The dimensions for the stator and four types of ducts namely cylindrical, profile, convergent, convergent-divergent with stators are given in table 1 and 2.

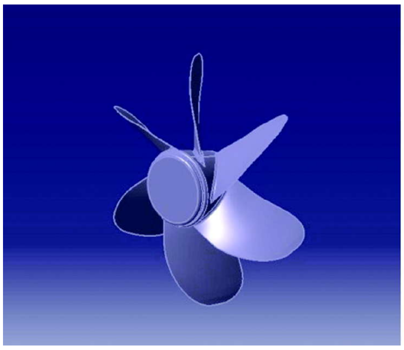

Fig. 1. Reference propeller

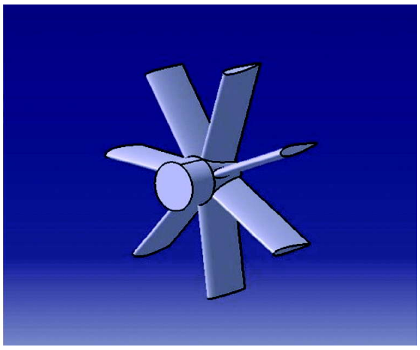

Fig. 2. Stator

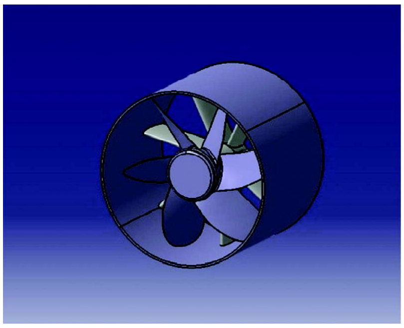

Fig. 3. Cylindrical duct

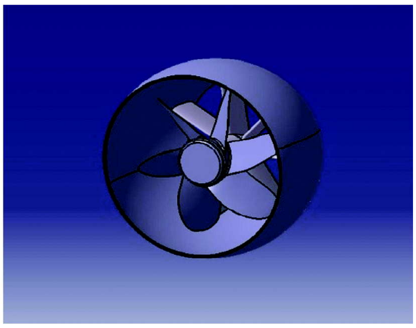

Fig. 4. Profile duct

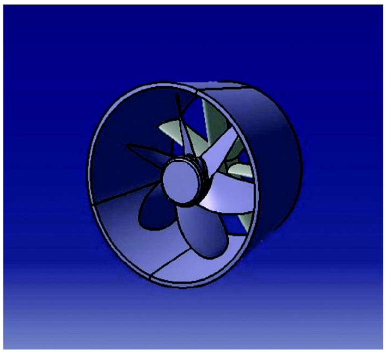

Fig. 5. Convergent duct

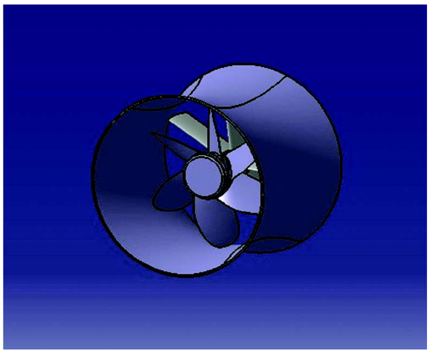

Fig. 6. Convergent-divergent duct

3.2 Dimensions of Stator

Table 1. Dimensions of Stator.

Number of blades	7
Blade Profile	NACA 0015
Diameter	389
Hub Diameter	80.4

3.3 Dimensions of Ducts

Table 2. Dimensions of Ducts.

Duct	**Inner radius (mm)**	**Outer radius (mm)**	**Length (mm)**	**Thickness (mm)**
Cylindrical	195.5	195.5	300	12
Profile	195.5	165	300	12
Convergent	230	165	300	12
Convergent-divergent	230	240	300	12

4. CFD ANALYSIS

The aim was to assess the importance of kind of ducts with stator to reduce the induced noise during the operation of propeller. This can lead to a reliable and versatile simulation setup which may be used for tests of different propeller ducts with stator and the selection of best duct with low sound pressure level.

To get better results the numerical simulations have been carried out with a finite volume module called FLUENT. In the CFD analysis, LES module turbulence model is used. Surfaces which can rotate relatively are defined as moving wall and are dependent on the fluid around them. Fluid Zone has to be considered as a cylinder extending either side of the bladed propeller. Cylinder walls are categorized as stationary wall and the inlet and outlet are defined as velocity inlet (7.08 m/sec) and outflow. Fluid zone in the inner volume is defined as moving mesh at 780 rpm in x-direction.

With this configuration CFD analysis is carried out on all the four kinds of ducted propellers with stator using large eddy simulation (LES).

Table 3. Details of non-cavitating flow.

Pressure link	Simple
Pressure	Standard
Discretization scheme for convective fluxes and turbulence parameters	Second Order Upwind
Turbulence model	Large Eddy Simulation
Near wall treatment	Standard Wall Functions
Solver	Unsteady

4.1 Meshing

ANSYS ICEM CFD meshing software has advanced CAD readers and repair tools to mesh the complex geometries. ICEM CFD numerical code is used for meshing in order to obtain grid independence.

The type of mesh used for this analysis is as follows

Elementtype : Unstructured tetrahedral

Order : Quadratic

The meshed models of all 6 bladed marine ducted propellers with stators are shown in the below figures 7 to 11.

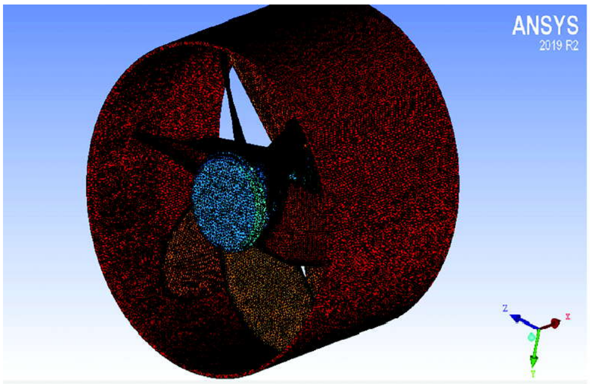

Fig. 7. Meshed cylindrical duct

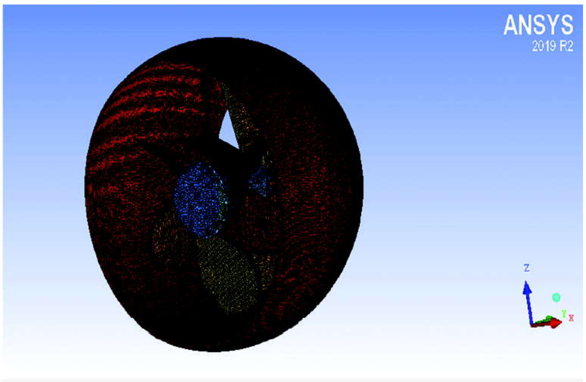

Fig. 8. Meshed profile duct

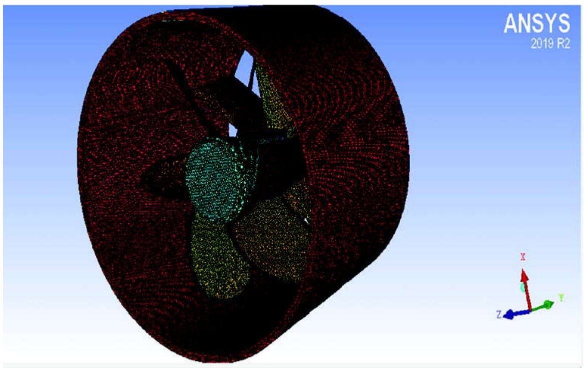

Fig. 9. Meshed convergent duct

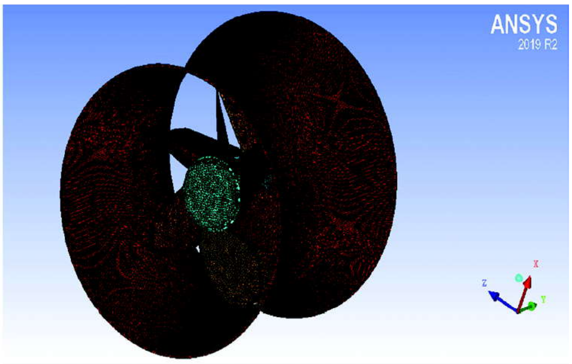

Fig. 10. Meshed convergent-divergent duct

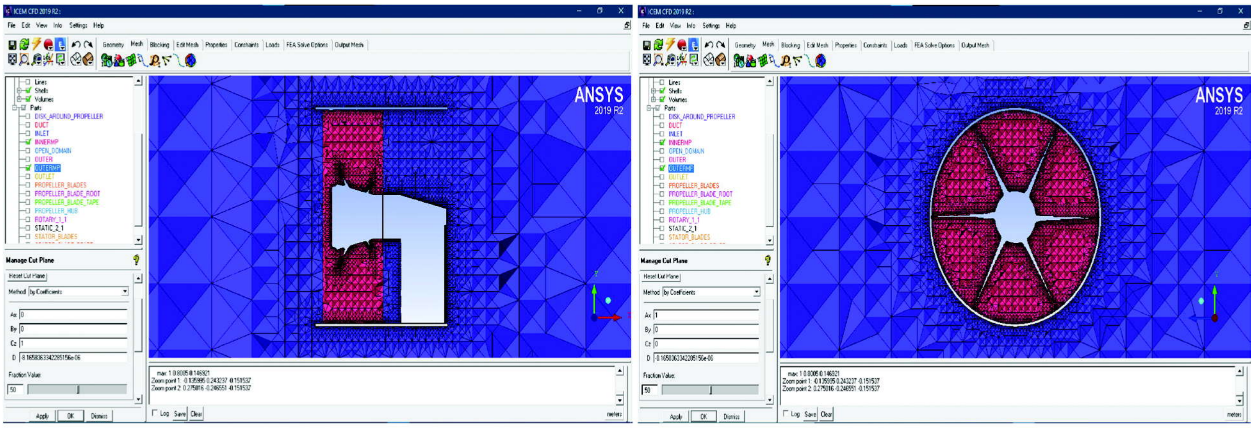

Fig. 11. Cut plane of inner and outer domain

4.2 *Calculation of Thrust and Torque Coefficients from ANSYS*

The force component *i.e.*, is directly obtained from the CFD analysis is considered as Thrust.

Thrust coefficient $K_T = T / \rho n^2 D^4$

Torque coefficient $K_Q = Q / \rho n^2 D^5$

Operating conditions required for solving Thrust coefficient and Torque coefficient :

Density of seawater (ρ) : 1029 kg/m^3

Diameter of propeller (D) : 0.389 m

Speed of the propeller (n) : 13 rps

Thrust and Torque values of Reference and 04 varieties of ducted Propellers with stators which were obtained from the CFD analysis is shown in Table 4

Table 4. Values of thrust and torque of ducted propellers with Reference propeller.

Parameter	Reference Propeller	Cylindrical duct with stator	Profile duct with stator	Convergent duct with stator	Convergent Divergent duct with stator
Thrust (N)	1385.73	2585	1888	6325	3099
Torque(N-m)	51.89	77	84	76	72

4.3 *Comparison of Thrust and Torque coefficients*

Using the above, Thrust and Torque coefficients are calculated for ducted propeller with stators and reference propeller. A Comparison of Thrust coefficient and Torque coefficients is shown in Table 5.

Table 5. Comparison of thrust and torque coefficients of ducted propellers with stator and Reference propeller.

Parameter	Reference Propeller	Cylindrical duct with stator	Profile duct with stator	Convergent duct with stator	Convergent Divergent duct with stator
Thrust coefficient	0.348	0.649	0.474	1.588	0.778
Torque coefficient	0.0335	0.049	0.054	0.049	0.046

From the above table, Thrust and Torque coefficients are increased for cylindrical ducted propeller with stator compared to reference propeller. Even though Convergent and Convergent Divergent ducted propellers with stator have higher Thrust coefficient, lower noise is from cylindrical ducted propeller while satisfying required Thrust and torque.

5. ACOUSTIC ANALYSIS

The output of CFD results is carried further for Acoustic analysis. Acoustic analysis was done in ANSYS using Ffowcs Williams-Hawkings (FW-H) formulation. The sound pressure level was predicted over the frequency range of 0-2 kHz for 6 bladed propeller with four different kinds of ducts with stator. Receiver is placed at 1m. Reference pressure is taken as 1e-06. Noise spectra for cylindrical ducted propeller with stator is shown in Fig. 12.

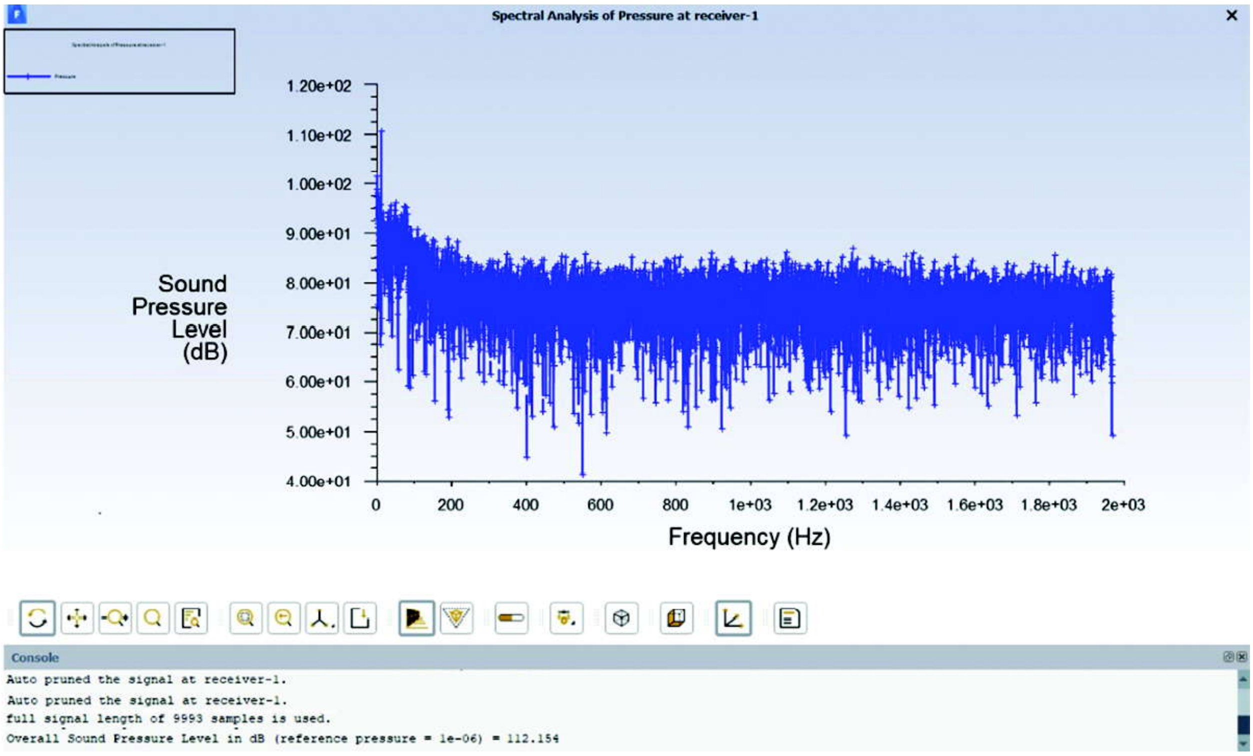

Fig. 12. Frequency vs sound pressure level graph of cylindrical ducted propeller with stator

5.1 *Comparison of Sound pressure level (SPL) of ducted propellers*

Sound Pressure level (SPL) of all 6 bladed propeller with four kinds of ducts with stators are given in Table 6.

It can be seen from table 6, compared to reference propeller, all ducted propellers provide lesser noise but cylindrical ducted propeller with stator provide least noise among studied configurations.

6. CONCLUSION

The Non-Cavitating noise of underwater marine propeller has been carried out by numerical method. The numerical investigation of turbulent flow is carried out using Large Eddy Simulation (LES) approach in CFD analysis and using Ffowcs Williams -Hawkings (FW-H) in computational acoustic analysis to find overall Sound Pressure Level (SPL) of a propeller with duct and stator at rotational speed of 780 rpm and flow velocity at 7.08 m/s. From the analysis, it is seen that propeller with cylindrical duct with stator generates less noise of 112.22 dB than Profile duct with stator, Convergent duct with stator and Convergent divergent duct with stator. Thrust and Torque coefficients are better for cylindrical ducted propeller compared to reference propeller thereby implying that cylindrical ducted propeller with stator is optimum choice.

7. ACKNOWLEDGEMENTS

The authors wish to express their sincere gratitude to Dr. Y. Sreenivas Rao, outstanding scientist and Director, NSTL Visakhapatnam and Sri PVS Ganesh Kumar outstanding scientist for permitting to publish this paper.

8. REFERENCES

[1] Santhosh Babu K.P. and Padmanabhan S., 2017. "design of marine propeller blade with different blade sequences analyse the hydro for mation under pressure hydrodynamic fill", **12**(17).

[2] Bontempo R. and Manna M., 2018. "Performance analysis of ducted marine propellers. Part-II Accelerating duct", **75,** 153-164.

[3] Mehdi Chamanara, Hassan Ghassemi, Manouchehr Fadavie and Mohammad Aref Ghassemi, 2017. "Effects of the duct angle and propeller location on the hydrodynamic characteristics of the ducted propeller".

[4] Tadeusz Koronowicz, Zbigniew Krzemianowski, Teresa Tuszkowska and Jan A. Szantyr, 2009. "A complete design of ducted propellers using the new computer system", **16,** 34-39.

[5] João Manuel Baltazar , Douwe Rijpkema, José Falcão de Campos and Joha Bosschers, 2018. "Prediction of the Open Water Performance of Ducted Propellers with a Panel Method".

[6] Negin Donyavizadeh and Parviz Ghadimi, 2020. "Efficacy Analysis of Thickness and Camber Size of Cross Section of the Stator on Hydrodynamic Parameters in Linear Jet Propulsion System," Hindawi Mathematical Problems in Engineering, ID 5861948.

The Journal of Acoustical Society of India : Vol. 49, No. 1-2, 2022 (pp. 36-47)

Evaluation and analysis of Kirkwood-Buff integrals of 1, 4-dioxane + aromatic hydrocarbon binary mixtures using inversion procedure and regular solution theory from ultrasonic speed and density data

Anil Kumar Nain[1*] and Dinesh Chand[2]

[1]*Department of Chemistry, Dyal Singh College (University of Delhi), New Delhi-110 003, India*

[2]*Department of Chemistry, Amity University Dubai Campus, Dubai International Academic City, Dubai, UAE*

e-mail: ak_nain@yahoo.co.in

[Received: 15-01-2021; Accepted: 10-08-2021]

ABSTRACT

The Kirkwood-Buff (K-B) theory can be used to characterize the intermolecular interactions in liquid mixtures. The interactions are characterized by the K-B parameters, G_{AA}, G_{BB} and G_{AB}, which reflect interaction between like-like and like-unlike species in the mixture. The experimental ultrasonic speed and density data of 1, 4-dioxane + benzene/toluene/*o*-xylene/*m*-xylene/*p*-xylene/mesitylene binary mixtures at 298.15 K have been used to calculate the K-B integrals by using the inverse procedure and regular solution theory. This procedure utilizes experimental thermodynamic properties of mixtures, *viz.*, partial molar volume, isothermal compressibility, excess free energy and partial vapour pressure. The K-B parameter, G_{AB} obtained using this procedure indicated that the correlation/interaction between 1, 4-dioxane and aromatic hydrocarbon molecules follow the order: benzene > toluene > *p*-xylene > *m*-xylene > *o*-xylene > mesitylene, which is found in good agreement with the trends exhibited by the excess properties of these mixtures obtained experimentally.

1. INTRODUCTION

The physicochemical and thermodynamic properties of liquid mixtures provide valuable information regarding intermolecular interactions between the component molecules[1-4], which is of significance in many theoretical and applied areas of research and such proprties are regularly required in designing many chemical and industrial processes[5-8]. Although there exists a large amount of experimental data on the physicochemical, thermodynamic, transport, acoustic and spectroscopic properties of liquid systems in the literature[9-18], but in comparison, there exists very few theoretical reports on the elucidation of molecular structure and valuation of thermodynamic properties of liquid mixtures using the existing theories of solutions. The researchers in this area have focused their interest significantly on the molecular structure along with some representative macroscopic properties that assists to characterize it. The theoretical prediction of physicochemical properties of liquid systems comprises an interdisciplinary interest and proved to be an excellent qualitative and quantitative tool for explaining the molecular structure and nature and extent of interaction in liquid systems.

Kirkwood & Buff[19] theory of solutions relate the radial distribution functions of various molecular species in a mixture to the derivatives of their thermodynamic properties. This is a general statistical mechanical theory of solutions, which is valid both classically and quantum mechanically and is applicable to all types of intermolecular interactions. Also, it is one of the most recognized theories of solutions that directly relate the thermodynamic quantities with the solution structure without any assumptions. K-B theory, being a powerful liquid state theory, has not received considerable attention in thermodynamic literature, as it should get. Only few examples of practical applications[20-38] to aqueous binary mixtures can be found in which this theory has been to be used for aqueous-alcohol[20-28] binary mixtures, aqueous solutions containing electrolytes[29,30] and aqueous solutions containing amino acids[31,32]. To the best of our knowledge, very few studies have been made in the literature on non-aqueous binary mixtures[33-38]. The main objective of the present study is to apply the K-B theory to binary solvent systems of varied nature in order to extract new information on the interactions between the species existing in these systems on molecular level. In this paper, the K-B theory has been extended to binary mixtures of 1, 4-dioxane with benzene, toluene, *o*-xylene, *m*-xylene, *p*-xylene and mesitylene at 298.15 K and at atmospheric pressure. Some new routes for predicting various parameters/terms involved in K-B theory have also been incorporated and effectively used. The experimental data required for the calculations have been taken from our previous studies[39,40].

2. THEORY

The solution theory proposed by Kirkwood and Buff[19] contains the theory of the grand ensembles on the one hand to relate compositional fluctuations to the derivatives of the chemical potentials of the components and then relate them to the integrals of the radial distribution functions of the several type of molecular pairs of species present in the solution. The K-B theory defines thermodynamic properties of a solution over the whole concentration range using the values of G_{AB}, expressed as K-B integrals, given by

$$G_{\mathrm{AB}} = \int_0^\infty [g_{\mathrm{AB}}(r) - 1] 4\pi r^2 dr \tag{1}$$

where g_{AB}(r) is the angle averaged pair correlation function. The integral extends over the whole range of intermolecular distances between the pair of molecules of species A and B. The interpretation of these parameters is best obtained by considering the product of number density, ρ and G_{AB}, *i.e.*, $\rho_A G_{AB}$ or $\rho_A[g_{AB}(r) - 1]\, 4\pi r^2 dr$, where ρ_A is the number density of the A species[20]. The quantity G_{AB} conveys information of the average affinity of the A molecules towards B molecules and *vice-versa*. In the present study we have incorporated a new method, in the inversion procedure proposed by Ben-Naim[20], for the computation of partial vapour pressures of the mixtures for which these vapour pressure data are not available. The composition dependence of G_{AB} values provide valuable insight into the molecular structure and nature of interactions in the multi-component liquid mixture.

2.1 *The inversion procedure to compute G_{AB}'s*

The K-B equations[19,20] for the binary mixture of species A and B can be written as :

$$\eta = \rho_{\mathrm{A}} + \rho_{\mathrm{B}} + \rho_{\mathrm{A}}\rho_{\mathrm{B}}(G_{\mathrm{AA}} + G_{\mathrm{BB}} - 2G_{\mathrm{AB}}) \tag{2}$$

$$\xi = 1 + \rho_{\mathrm{A}}G_{\mathrm{AA}} + \rho_{\mathrm{B}}G_{\mathrm{BB}} + \rho_{\mathrm{A}}\rho_{\mathrm{B}}(G_{\mathrm{AA}}G_{\mathrm{BB}} - G_{\mathrm{AB}}^2) \tag{3}$$

where η and ζ are constants, ρ_A and ρ_B are the number densities of A and B, respectively. The calculations of various terms involved in equations (2) and (3) were done by using the relations given in the literature[20,31]. The derivatives of the chemical potentials were obtained using the vapour pressure data, assuming that the vapour above the mixture at room temperature as an ideal gas. Thus, for component A, we can write

$$\mu_{\mathrm{A}} = \mu_{\mathrm{A}}^{\mathrm{o}} + kT \ln P_{\mathrm{A}} \tag{4}$$

where P_{A} is the partial pressure of component A over the given mixture of A and B. If x_A is the mole fraction of A in the mixture, then we get the relation

$$x_{\mathrm{A}} \left(\frac{\partial p_{\mathrm{A}}}{\partial x_{\mathrm{A}}} \right) = \frac{\rho^{*}}{\eta} \tag{5}$$

The number density, ρ^* of the mixture is calculated from the partial molar volumes, $\overline{V}_{\mathrm{m,A}}$ and $\overline{V}_{\mathrm{m,B}}$ of the components A and B, respectively, in the mixtures.

$$\rho^{*} = \rho_{\mathrm{A}} + \rho_{\mathrm{B}} = (x_{\mathrm{A}} \overline{V}_{\mathrm{m,A}} + x_{\mathrm{B}} \overline{V}_{\mathrm{m,B}})^{-1} \tag{6}$$

The values of $\overline{V}_{\mathrm{m,A}}$ and $\overline{V}_{\mathrm{m,B}}$ in the mixtures are calculated from the experimental density data by using the procedure described elsewhere[41].

From equation (5) we can obtain η from the data on partial vapour pressures of either A or B in the entire composition range. The partial vapour pressures are calculated from the activity coefficients, which are related to the excess Gibbs free energy of the mixture. The excess free energy of mixtures is given as

$$G^{\mathrm{E}} = H^{\mathrm{E}} - TS^{\mathrm{E}} \tag{7}$$

The excess enthalpies, H^E and excess entropies, $-S^E$ are calculated from the internal pressures, π_{i} and free volumes, V_{f} of the mixtures by using the modified relations from regular solution theory proposed by Hildebrand *et al.*[42,43].

$$H^{\mathrm{E}} = \pi_i V_{\mathrm{m}} - \left[x_A \pi_{i,\mathrm{A}} V_{\mathrm{m,A}} + x_{\mathrm{B}} \pi_{i,\mathrm{B}} V_{\mathrm{m,B}} \right] \tag{8}$$

$$-S^{\mathrm{E}} = R \left[x_A \ln V_{\mathrm{f,A}} + x_{\mathrm{B}} \ln V_{\mathrm{f,B}} - \ln V_{\mathrm{f,m}} \right] \tag{9}$$

where π_{i} of the mixtures are calculated using the thermodynamic equation of state

$$\pi_i = \left(\frac{\partial E}{\partial V} \right)_T = T \left(\frac{\partial P}{\partial T} \right)_V - P = T \left(\frac{\alpha_p}{k_T} \right) - P \tag{10}$$

where α_p is the isobaric expansivity of the mixture evaluated from temperature dependence of density data[39] using the following relation

$$\alpha_{\mathrm{p}} = \left(-1/\rho \right) \left(\partial \rho / \partial T \right)_{\mathrm{p}} \tag{11}$$

For most of the liquids, the thermal pressure coefficient multiplied by absolute temperature, *i.e.*, $T(\alpha_p/k_T)$ is very high so that the external pressure P becomes negligible in comparison[44,45], therefore it may be neglected in the equation (10) in the present calculations. The V_{f} of the mixtures are calculated from the relation[42,43].

$$V_{\mathrm{f}} = \frac{RT}{(P + \pi_i)} \tag{12}$$

since P is very small as compared to π_{i}, it has been neglected in the equation (12) in the present calculations. These systems can be considered as 'regular' mixtures, as the S^E values obtained using equation (9) for these mixtures are very low ($S^{\mathrm{E}} \approx 0$), for which G^E is given by

$$G^{\mathrm{E}} = x_{\mathrm{A}} x_{\mathrm{B}} N w \tag{13}$$

where w is a constant computed from equation (13), which may depend on temperature but is independent of composition. The activity coefficients in a regular mixture are given by

$$\ln \gamma_i = (1 - x_i)^2 w / kT \tag{14}$$

The partial vapour pressures of the components in the mixtures were calculated using the activity coefficients. Using the mole fraction dependence of partial vapour pressure of either A or B, η over the entire composition range can be obtained from equation (5). The vapour pressures of the liquids have been taken from the literature[46-48]. The isothermal compressibility, k_T, is calculated using the well-known thermodynamic relation

$$k_{\mathrm{T}} = k_{\mathrm{s}} + \frac{TV\alpha_T^2}{C_{\mathrm{p}}} \tag{15}$$

where k_{s} is isentropic compressibility and C_{p} is the heat capacity. The C_{p} values for pure liquids have been taken from literature[49] and the mixtures have been calculated by using the relation

$$C_{\mathrm{p}} = x_{\mathrm{A}} C_{\mathrm{p,A}} + x_{\mathrm{B}} C_{\mathrm{p,B}} \tag{16}$$

Using the values of η, ζ, $\overline{V}_{\mathrm{m,A}}$ and $\overline{V}_{\mathrm{m,B}}$, the G_{AB} is calculated using the relation

$$\overline{V}_{\mathrm{m,A}} \overline{V}_{\mathrm{m,B}} = (\xi - \eta G_{\mathrm{AB}}) / \eta^2 \tag{17}$$

Once G_{AB} is obtained, the values of G_{AA} and G_{BB} can be easily calculated using the relations given in the literature[20,31].

Another quantity proposed by Ben-Naim, Δ_{AB}, which is a measure of the "degree of similarity" between the two components of the mixture[20], has also been calculated by using the equation given below

$$\Delta_{\mathrm{AB}} = G_{\mathrm{AA}} + G_{\mathrm{BB}} - 2G_{\mathrm{AB}} \tag{18}$$

The condition $\Delta_{\mathrm{AB}} = 0$ signifies symmetrical ideal solutions. The magnitude of Δ_{AB} can be used to specify the extent of deviation from ideal behaviour of solution.

3. RESULTS AND DISCUSSION

The values of K-B parameters for the above-mentioned binary systems have been calculated as a function of mole fraction, x_{A} of component A (1,4-dioxane) at 298.15 K using the above procedure. The values of various parameters of pure liquids required for the calculations are listed in Table 1. The values of K-B parameters, *viz.*, G_{AA}, G_{BB}, G_{AB} and Δ_{AB} along with some other parameters for the binary systems

Table 1. Values of ρ, u, p, ks, k_T, α_{p}, and C_{p} for pure liquids at 298.15 K used in the calculation of K-B integrals.

Liquid	ρ (kg m^{-3})	u (m s^{-1})	p (N m^{-2})	k_{s} (10^{-10} m^2 N^{-1})	k_{T} (10^{-10} m^2 N^{-1})	α_{p} (10^{-3} K^{-1})	C_{p} (J mol^{-1})
1,4-Dioxane	1027.95	1344.7	9288.1	5.380	6.231	0.706	149.8
Benzene	1027.95	1299.5	12685.8	6.778	10.393	1.362	136.8
Toluene	862.36	1307.3	3794.5	6.785	9.209	1.094	157.3
o-Xylene	871.54	1347.5	880.0	6.290	8.130	0.973	186.1
m-Xylene	881.00	1323.6	1113.7	6.637	8.635	0.997	183.0
p-Xylene	891.55	1307.4	1186.7	6.828	8.925	1.015	181.5
Mesitylene	902.55	1339.8	322.3	6.467	8.108	0.909	209.3

investigated as function of mole fraction, x_A of 1,4-dioxane for these mixtures are listed in Table 2. The variations of G_{AA}, G_{BB}, G_{AB} and Δ_{AB} against mole fraction, x_A of 1,4-dioxane for each mixture are shown graphically in Figs. 1-6. The low values excess entropy ($S^E \approx 0$) obtained for these systems (Table 2) clearly indicate that these mixtures can be considered as regular solutions[43].

Table 2. Values of ρ, u, ρ^*, H^E, TS^E, $\ln(P_A)$, η, G_{AB}, G_{AA}, G_{BB} and Δ_{AB} for 1,4-dioxane + aromatic hydrocarbon binary mixtures at 298.15 K

x_A	ρ (kg m^{-3})	u (m s^{-1})	ρ^* (10^4 m^{-3})	H^E (J mol^{-1})	TS^E (J mol^{-1})	ln(P_A)	η (10^4 m^{-3})	G_{AB}	G_{AA} (10^{-4} m^3 mol^{-1})	G_{BB}	Δ_{AB}
				1,4-Dioxane + benzene							
0.0713	884.38	1304.0	1.1220	498.9	-38.7	6.237	2.6755	-2.044	-0.708	14.039	17.419
0.1403	894.85	1308.1	1.1254	929.2	-72.4	6.934	1.4863	-1.136	-0.796	0.578	2.054
0.2123	905.82	1312.5	1.1290	1332.1	-104.3	7.368	1.0872	-0.831	-0.863	-1.124	-0.324
0.2809	916.30	1316.5	1.1324	1656.0	-130.3	7.667	0.9141	-0.699	-0.924	-1.384	-0.909
0.3528	927.31	1320.5	1.1359	1927.1	-152.6	7.915	0.8245	-0.631	-0.989	-1.365	-1.092
0.4195	937.55	1324.0	1.1391	2109.2	-168.2	8.107	0.7901	-0.604	-1.049	-1.281	-1.122
0.5037	950.51	1328.2	1.1432	2238.0	-180.3	8.313	0.7976	-0.610	-1.117	-1.161	-1.057
0.5800	962.30	1332.0	1.1469	2256.7	-183.8	8.476	0.8560	-0.655	-1.144	-1.056	-0.890
0.6504	973.21	1335.1	1.1502	2168.2	-178.7	8.610	0.9740	-0.745	-1.069	-0.966	-0.545
0.7197	983.99	1337.5	1.1535	1964.7	-164.2	8.730	1.2059	-0.922	-0.686	-0.882	0.276
0.7822	993.74	1339.8	1.1565	1703.7	-144.4	8.831	1.6607	-1.270	0.643	-0.802	2.381
0.8561	1005.30	1342.0	1.1600	1267.6	-109.4	8.941	3.6479	-2.789	10.716	-0.648	15.646
				1,4-Dioxane + toluene							
0.0688	862.36	1308.4	0.9487	144.8	-15.0	6.201	2.3260	-2.133	-0.452	13.129	16.943
0.1373	871.54	1309.5	0.9619	267.6	-28.5	6.911	1.2863	-1.179	-0.727	-0.399	1.231
0.2112	881.00	1310.9	0.9766	383.3	-41.6	7.362	0.9386	-0.860	-0.856	-1.808	-0.945
0.2858	891.55	1312.4	0.9920	474.8	-52.6	7.686	0.7884	-0.722	-0.944	-1.867	-1.367
0.3552	902.55	1313.9	1.0067	536.4	-60.7	7.923	0.7241	-0.663	-1.011	-1.725	-1.411
0.4361	913.11	1315.9	1.0244	582.0	-67.4	8.150	0.7022	-0.643	-1.075	-1.535	-1.324
0.5064	925.82	1317.9	1.0403	597.6	-70.8	8.319	0.7206	-0.660	-1.107	-1.386	-1.174
0.5819	937.25	1320.4	1.0579	589.3	-71.5	8.479	0.7838	-0.718	-1.085	-1.251	-0.901
0.6506	949.92	1323.2	1.0744	563.8	-69.6	8.610	0.8994	-0.823	-0.927	-1.152	-0.432
0.7212	961.80	1326.3	1.0920	505.0	-63.8	8.733	1.1302	-1.034	-0.353	-1.075	0.641
0.7903	974.37	1329.8	1.1097	420.7	-54.4	8.843	1.6448	-1.505	1.746	-1.038	3.718
0.8640	987.06	1334.2	1.1291	301.9	-40.1	8.953	3.8978	-3.566	17.020	-1.167	22.986
				1,4-Dioxane + o-xylene							
0.0672	882.50	1341.5	0.8408	-123.7	5.8	6.177	2.0854	-2.189	-0.239	12.057	16.195
0.1391	890.29	1335.1	0.8589	-266.4	13.3	6.925	1.1259	-1.180	-0.686	-1.405	0.270
0.2103	898.42	1329.6	0.8776	-379.7	19.6	7.358	0.8391	-0.879	-0.853	-2.372	-1.468
0.2853	907.43	1324.8	0.8983	-467.6	24.9	7.684	0.7100	-0.743	-0.958	-2.257	-1.730
0.3543	916.23	1321.0	0.9183	-535.8	29.4	7.920	0.6579	-0.688	-1.027	-2.020	-1.672
0.4293	926.36	1317.9	0.9413	-582.9	32.9	8.133	0.6446	-0.673	-1.077	-1.776	-1.507
0.5092	937.85	1315.9	0.9671	-601.3	35.0	8.326	0.6716	-0.701	-1.088	-1.560	-1.246

Conted........

0.5810	948.83	1315.4	0.9917	-588.5	35.2	8.478	0.7380	-0.771	-1.017	-1.407	-0.882
0.6518	960.31	1316.2	1.0173	-550.3	33.8	8.612	0.8648	-0.903	-0.755	-1.292	-0.241
0.7248	972.90	1318.3	1.0453	-493.7	31.2	8.739	1.1259	-1.176	0.114	-1.221	1.244
0.7888	984.57	1321.9	1.0711	-407.0	26.2	8.841	1.6526	-1.726	2.754	-1.233	4.974
0.8595	998.21	1327.4	1.1012	-295.3	19.6	8.946	4.0766	-4.260	21.398	-1.625	28.294
1,4-Dioxane + m-xylene											
0.0938	870.79	1318.3	0.8335	-78.2	4.9	6.518	1.6772	-1.788	-0.371	3.949	7.154
0.1532	877.97	1315.4	0.8491	-121.1	7.8	7.025	1.1237	-1.197	-0.659	-1.430	0.306
0.2046	884.42	1313.2	0.8631	-154.0	10.2	7.329	0.9138	-0.973	-0.786	-2.173	-1.013
0.2698	892.98	1310.8	0.8816	-192.7	13.0	7.624	0.7754	-0.825	-0.891	-2.221	-1.461
0.3374	902.34	1308.8	0.9017	-229.7	15.8	7.866	0.7037	-0.748	-0.967	-2.045	-1.515
0.4002	911.47	1307.6	0.9212	-253.8	17.9	8.055	0.6750	-0.717	-1.017	-1.855	-1.438
0.4714	922.42	1307.0	0.9446	-272.7	19.6	8.238	0.6743	-0.716	-1.049	-1.661	-1.278
0.5487	935.04	1307.3	0.9714	-286.2	21.0	8.411	0.7094	-0.754	-1.032	-1.487	-1.012
0.6300	949.22	1309.1	1.0014	-281.2	21.2	8.572	0.7969	-0.847	-0.883	-1.348	-0.537
0.7182	965.73	1312.9	1.0362	-259.2	20.1	8.728	0.9942	-1.056	-0.263	-1.254	0.596
0.8035	982.98	1318.8	1.0725	-218.8	17.4	8.864	1.4422	-1.533	2.206	-1.258	4.014
0.8708	997.51	1325.5	1.1030	-164.4	13.3	8.963	2.4787	-2.635	11.920	-1.464	15.726
1,4-Dioxane + p-xylene											
0.0716	865.20	1305.1	0.8250	0.3	0.6	6.242	1.9676	-2.102	-0.225	9.693	13.673
0.1445	874.16	1303.2	0.8441	-0.9	1.3	6.964	1.0921	-1.166	-0.677	-1.649	0.007
0.2132	883.03	1301.9	0.8630	-3.0	2.0	7.372	0.8310	-0.887	-0.843	-2.433	-1.502
0.2871	893.05	1300.9	0.8844	-7.7	2.9	7.691	0.7070	-0.754	-0.950	-2.297	-1.739
0.3582	903.24	1300.5	0.9060	-14.9	3.8	7.932	0.6548	-0.698	-1.022	-2.045	-1.670
0.4358	915.03	1300.8	0.9309	-23.5	4.6	8.150	0.6428	-0.685	-1.071	-1.789	-1.490
0.5042	926.04	1301.8	0.9541	-31.1	5.3	8.315	0.6646	-0.708	-1.079	-1.601	-1.263
0.5846	939.81	1304.0	0.9830	-39.9	5.9	8.485	0.7348	-0.783	-0.997	-1.426	-0.858
0.6543	952.50	1307.0	1.0095	-44.8	6.1	8.617	0.8555	-0.911	-0.732	-1.314	-0.224
0.7249	966.15	1311.2	1.0380	-49.0	6.1	8.739	1.0910	-1.162	0.083	-1.248	1.160
0.7923	979.92	1316.6	1.0668	-47.4	5.7	8.846	1.5956	-1.700	2.738	-1.265	4.874
0.8623	995.15	1323.9	1.0985	-39.4	4.5	8.950	3.5679	-3.803	18.917	-1.630	24.892
1,4-Dioxane + mesitylene											
0.0696	868.20	1333.4	0.7360	-198.7	13.2	6.213	1.7898	-2.170	0.016	8.674	13.031
0.1408	875.52	1327.5	0.7568	-372.2	25.7	6.937	0.9939	-1.204	-0.609	-2.492	-0.693
0.2098	883.10	1322.1	0.7783	-530.3	37.5	7.355	0.7534	-0.911	-0.827	-3.037	-2.042
0.2800	891.32	1317.1	0.8015	-673.6	49.0	7.664	0.6459	-0.780	-0.950	-2.746	-2.136
0.3558	900.93	1312.5	0.8282	-799.3	59.9	7.925	0.5970	-0.720	-1.031	-2.365	-1.955
0.4276	910.83	1308.9	0.8554	-894.8	68.7	8.128	0.5892	-0.710	-1.070	-2.056	-1.705
0.5066	922.67	1306.0	0.8877	-968.5	76.4	8.320	0.6168	-0.743	-1.055	-1.786	-1.355
0.5801	934.74	1304.5	0.9202	-1004.1	81.1	8.476	0.6823	-0.821	-0.935	-1.597	-0.889
0.6548	948.06	1304.7	0.9559	-991.1	82.2	8.618	0.8108	-0.976	-0.560	-1.462	-0.070
0.7227	961.28	1306.5	0.9910	-940.2	79.6	8.735	1.0358	-1.247	0.405	-1.403	1.496
0.7936	976.27	1310.8	1.0306	-825.2	71.5	8.848	1.5719	-1.893	3.786	-1.468	6.104
0.8663	993.00	1318.5	1.0747	-627.7	55.8	8.956	3.9283	-4.732	26.730	-2.190	34.005

Figure 1(a) indicates the behavior of 1,4-dioxane-1,4-dioxane affinity over the entire composition range. Table 2 and Fig. 1(a) indicate that G_{AA} values are negative and decreases initially with increase in mole fraction till $x_A \approx 0.58$ and then increases after this mole fraction and finally become positive, suggesting decreasing correlation between 1,4-dioxane molecules and this correlation increases sharply after $x_A \approx 0.72$. Fig. 1(b) indicates that G_{BB} values are positive and decrease sharply with increase in mole fraction till $x_A \approx 0.21$, become negative after this concentration, and then increases slightly after this point, suggesting decreasing correlation between benzene molecules on increasing the amount of 1,4-dioxane in the mixture, which leads to disruption of the orientational order[50] present in benzene. Fig. 1(c) indicates that that G_{AB} values are negative and increase initially and exhibit a maximum at $x_A \approx 0.58$ and then decrease with increase in mole fraction of 1,4-dioxane, suggesting increasing correlation between 1,4-dioxane and benzene molecules due to the electron donor-acceptor type interactions[51] between electronegative oxygen atoms of 1,4-dioxane (as donor) and the π-electrons of ring of benzene molecules (as acceptor) at near equimolar concentration range $0.3 < x_A < 0.72$. Further, on increasing the amount of 1,4-dioxane in the mixture after $x_A \approx 0.72$, G_{AB} then decreases sharply with further increase in mole fraction of 1,4-dioxane. This behaviour is in agreement with the conclusions drawn in our earlier study[39,40], wherein V_m^E and κ_s^E vs. x_A curves exhibited a minimum at $x_A \approx 0.55$, indicating maximum interaction between 1,4-dioxane and benzene molecules around this composition. Figure 1(d) indicates that Δ_{AB} values are positive and decrease initially to negative values exhibiting a minimum at $x_A \approx 0.35$ and then again increase to positive values, indicating the dissimilarity between unlike molecules in the mixtures and negative deviations from the ideal behaviour[20].

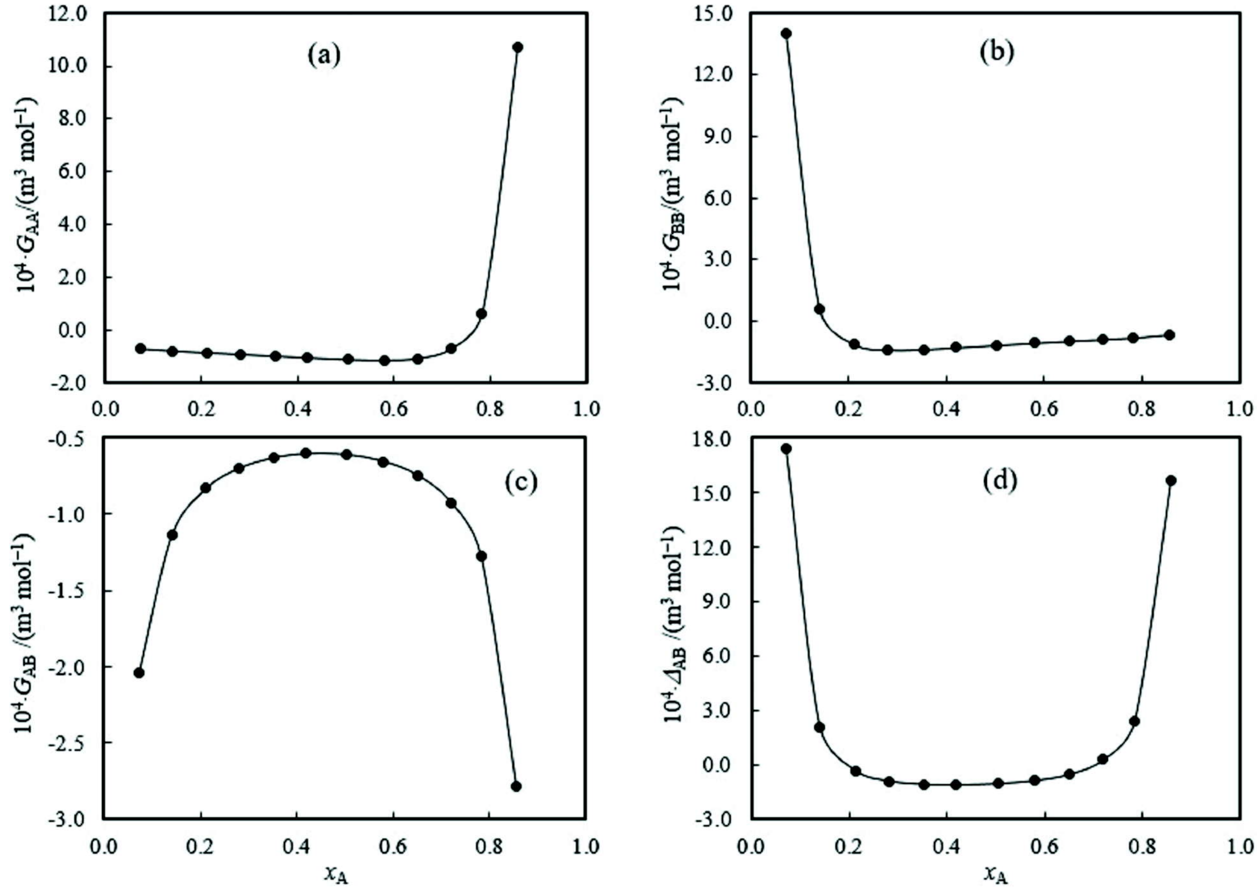

Fig. 1. Plots of G_{AA}, G_{BB}, G_{AB}, and Δ_{AB} against mole fraction, x_A of 1,4-dioxane for 1,4-dioxane + benzene mixtures at 298.15 K.

Figures 2-6 indicate that similar trends in G_{AA}, G_{BB}, G_{AB} and Δ_{AB} values (as above for 1,4-dioxane + benzene) against mole fraction, x_1 are exhibited by 1,4-dioxane + toluene/*o*-xylene/*m*-xylene/*p*-xylene/mesitylene mixtures also due to same reasons as discussed above for 1,4-dioxane + benzene mixtures. A close perusal of Table 2 indicates that the magnitude of G_{AB} varies in the order: benzene > toluene > *p*-xylene > *m*-xylene > *o*-xylene > mesitylene. This suggests that the affinity or interactions between the 1,4-dioxane and these aromatic hydrocarbon molecules follows the order: benzene > toluene > *p*-xylene > *m*-xylene > *o*-xylene > mesitylene. This may be due to the fact that the number of CH_3 groups substituted on the ring increase from benzene (with no substituted CH_3 group) to mesitylene (with three substituted CH_3 groups). Because methyl group (CH_3) being an electron-releasing group, would enhance the electron density of the benzene ring of the aromatic molecules, thereby decreasing the electron-accepting tendency of the aromatic ring, as we move from benzene to mesitylene, resulting in decreased donor-acceptor interaction between unlike molecules with increase in number of methyl group (CH_3) in the aromatic hydrocarbon molecule. The results and conclusions from K-B integrals are in good agreement with the conclusions drawn regarding the intermolecular interactions from the trends exhibited by the excess functions of these mixtures[39,40].

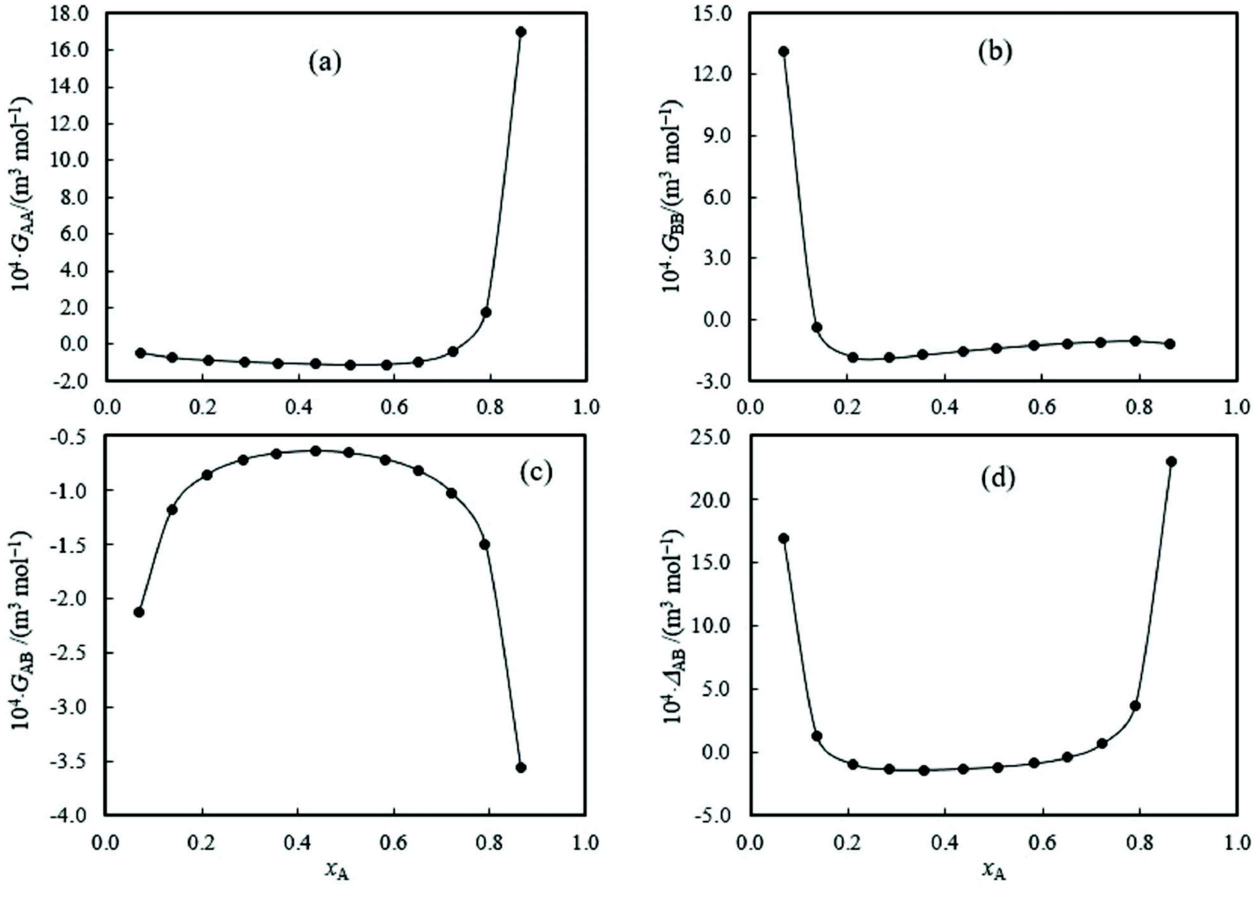

Fig. 2. Plots of G_{AA}, G_{BB}, G_{AB}, and Δ_{AB} against mole fraction, x_A of 1,4-dioxane for 1,4-dioxane + toluene mixtures at 298.15 K.

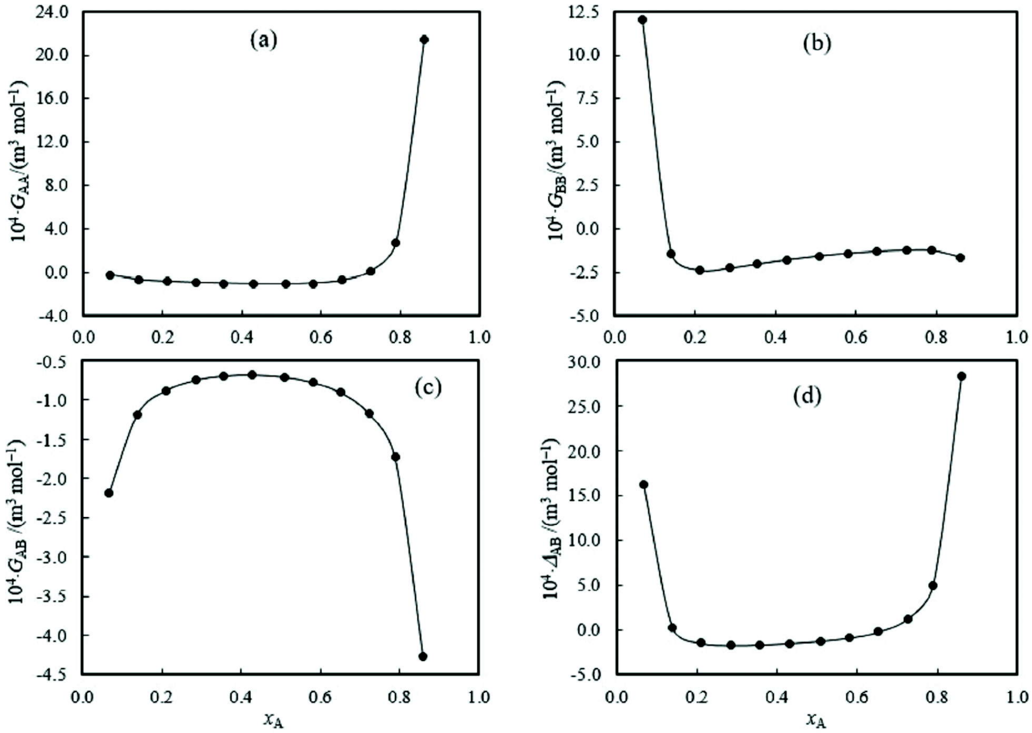

Fig. 3. Plots of G_{AA}, G_{BB}, G_{AB}, and Δ_{AB} against mole fraction, x_A of 1,4-dioxane for 1,4-dioxane + *o*-xylene mixtures at 298.15 K.

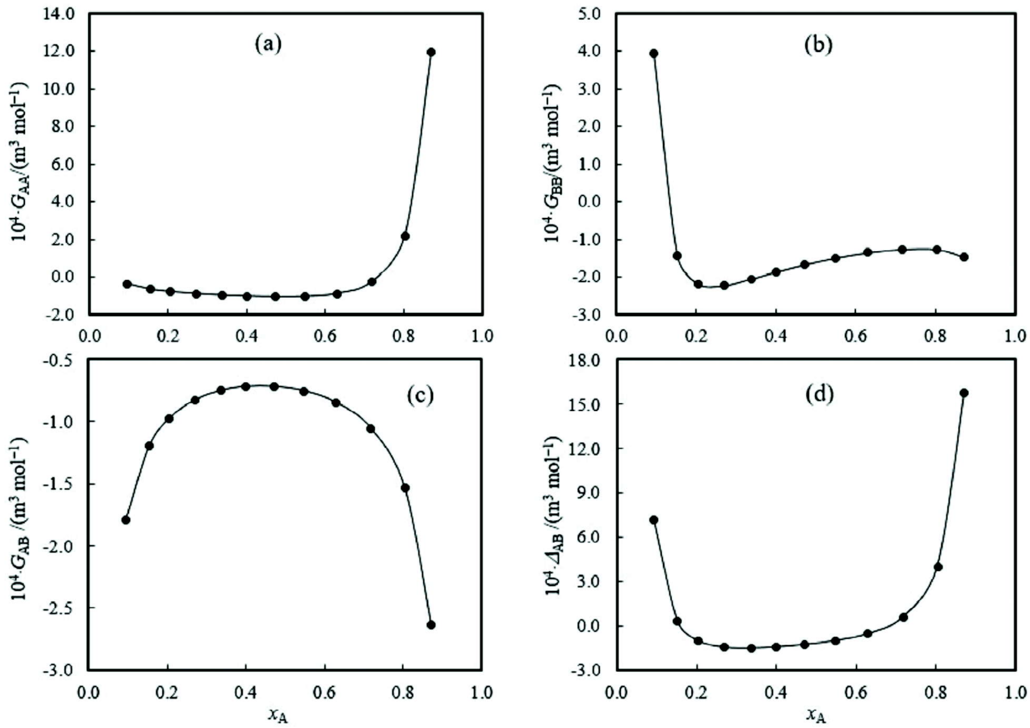

Fig. 4. Plots of G_{AA}, G_{BB}, G_{AB}, and Δ_{AB} against mole fraction, x_A of 1,4-dioxane for 1,4-dioxane for 1,4-dioxane + *m*-xylene mixtures at 298.15 K.

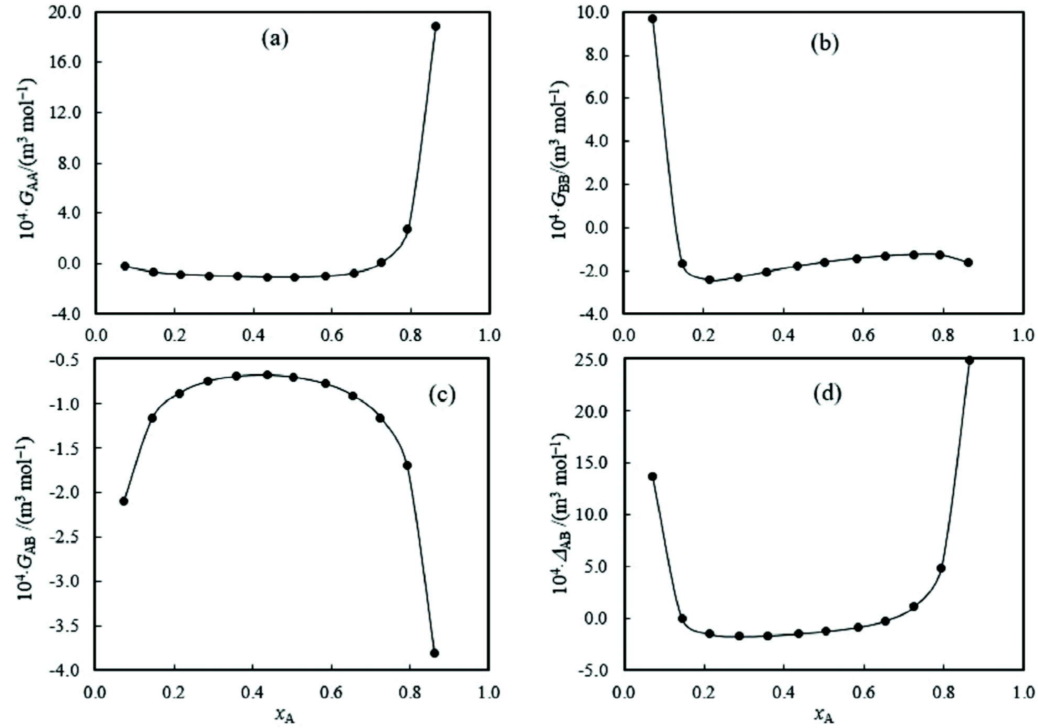

Fig. 5. Plots of G_{AA}, G_{BB}, G_{AB}, and Δ_{AB} against mole fraction, x_A of 1,4-dioxane for 1,4-dioxane + *p*-xylene mixtures at 298.15 K.

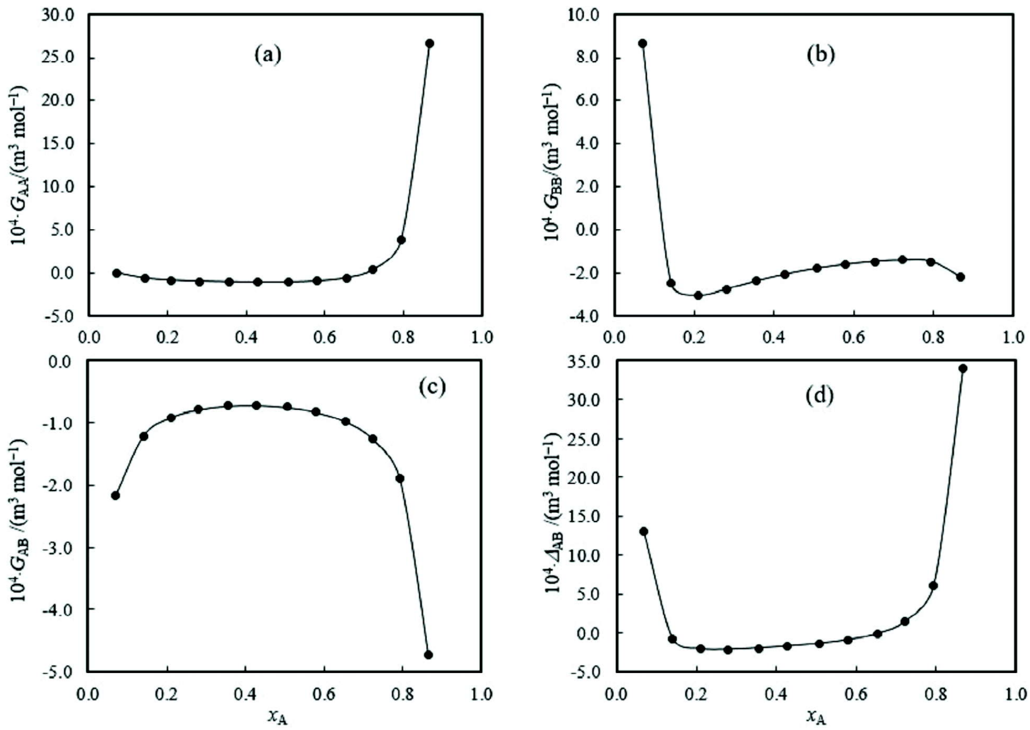

Fig. 6. Plots of G_{AA}, G_{BB}, G_{AB}, and Δ_{AB} against mole fraction, x_A of 1,4-dioxane for 1,4-dioxane + mesitylene mixtures at 298.15 K.

4. ACKNOWLEDGEMENTS

The author AKN is thankful to the Principal, Dyal Singh College (University of Delhi), New Delhi for encouragement and providing facilities.

5. REFERENCES

[1] Mrad S., Lafuente C., Giner B. and Hichria M., 2017. Thermochim. *Acta,* **655,** 169.
[2] Chaudhary N. and Nain, A.K., 2020. *J. Chem. Eng. Data,* **65,** 1447.
[3] Chaudhary N. and Nain A.K., 2020. *J. Mol. Liq.,* **297,** 111890.
[4] Romero C.M., Guzman C., Gascon I., Cea P. and Lopez M.C., 2006. *Int. J. Thermophys.,* **27,** 760.
[5] Nain A.K., Droliya P. and Gupta J., 2018. *Indian. J. Chem. A.,* **57,** 761.
[6] Dubey G.P., Rani S. and Kaur P., 2016. *J. Mol. Liq.,* **222,** 415.
[7] Kumar S., Lin W., Lee Y., Yadav J.S., Sharma D., Sharma V.K. and Moon I., 2010. *J. Mol. Liq.,* **155,** 8.
[8] Bahadur I., Deenadayalu N. and Ramjugernath D., 2014. *Thermochim. Acta,* **577,** 87.
[9] Rani R. and Bhatia S.C., 2013. *J. Chem. Thermodyn.,* **58,** 254.
[10] Bhalodia J. and Sharma S., 2013. *J. Solut. Chem.,* **42,** 1794.
[11] Nain A.K., 2006. *Bull. Chem. Soc. Jpn.,* **79,** 1688.
[12] Nain A.K., 2016. *J. Mol. Liq.,* **224,** 1055.
[13] Droliya P. and Nain A.K., 2017. *J. Mol. Liq.,* **241,** 549.
[14] Droliya P. and Nain A.K., 2018. *J. Chem. Thermodyn.,* **123,** 123.
[15] Droliya P. and Nain A.K., 2019. *J. Chem. Thermodyn.,* **132,** 142.
[16] Chaudhary N. and Nain A.K., 2020. *J. Mol. Liq.,* **305,** 112816.
[17] Ali A. and Nain A.K., 1997. *Indian J. Pure. Appl. Phys.,* **35,** 729.
[18] Ali A., Nain A.K., Sharma V.K. and Ahmad S., 2004. *Indian J. Pure Appl. Phys.,* **42,** 666.
[19] Kirkwood J.G. and Buff F.P., 1951. *J. Chem. Phys.,* **19,** 774.
[20] Ben-Naim A., 1977. *J. Chem. Phys.,* **67,** 4884.
[21] Shuglin I.L. and Ruckenstein E., 2006. *J. Phys. Chem. B.,* **110,** 12707.
[22] Perera A., Sokolic F., Almasy L. and Koga Y., 2006. *J. Chem. Phys.,* **124,** 124575:1.
[23] Gonzalez J.A., Mozo I., Villa S., Riesco N., De La Fuente I.G. and Cobos J.C., 2006. *J. Solut. Chem.,* **35,** 787.
[24] Newman K.E., 1994. *Chem. Soc. Rev.,* **23,** 31.
[25] Newman K.E., 1988. *J. Chem. Soc., Faraday Trans.,* **84,** 3885.
[26] Vergara A., Paduano L., Capuano F. and Sartorio R., 2002. *Phys. Chem. Chem. Phys.,* **4,** 4716.
[27] Zielkiewicz J., 1998. *J. Chem. Soc., Faraday Trans.,* **94,** 1713.
[28] Banerjee D., Laha A.K., Chatterjee P. and Bagchi S., 1995. *J. Solut. Chem.,* **24,** 301.
[29] Covington A.K. and Newman K.E., 1988. *J. Chem. Soc., Faraday Trans.,* **84,** 1393.
[30] Pierce V., Kang M., Aburi M., Weerasinghe S. and Smith P.E., 2008. *Cell. Biochem. Biophys.,* **50,** 12984.
[31] Bisht Y. and Nain A.K., 2019. *Indian J. Chem. A,* **58,** 281.
[32] Nain A.K., Droliya P. and Gupta J., 2017. *Indian J. Chem. A,* **56,** 939.
[33] Pandey J.D. and Verma R., 2001. *Chem. Phys.,* **270,** 429.
[34] Guha A. and Ghosh N.K., 2006. *Indian J. Chem. A,* **45,** 593.

[35] Nain A.K., 2009. *J. Chem. Sci.,* **121,** 361.
[36] Nain A.K., 2008. *J. Solut. Chem.,* **37,** (2008) 1541.
[37] Matteoli E., 1997. *J. Phys. Chem. B,* **101,** 9800.
[38] Marcus Y., 2006. *J. Solut. Chem.,* **35,** 251.
[39] Nain A.K., Chandra P., Pandey J.D. and Gopal S., 2008. *J. Chem. Eng. Data,* **53,** 2654.
[40] Nain A.K., Chaudhary N., Ankita Gupta J. and Chandra P., 2017. *J. Chem. Thermodyn.,* **108,** 145.
[41] Chaudhary N. and Nain A.K., 2018. *J. Mol. Liq.,* **271,** 501.
[42] Hildebrand J.H. and Scott R.L., 1962. Regular solutions, Prentice Hall, Englewood Cliffs, New Jersey.
[43] Hildebrand J.H., 1947. *J. Chem. Phys.,* **15,** 225.
[44] Dack M.R.J., 1975. *Chem. Soc. Rev.,* **4,** 211.
[45] Pal A. and Kumar H., 2004. *Indian J. Chem. A,* **43,** 34.
[46] Crenshaw J.L., Cope A.C., Finkelstein N. and Rogan R., 1938. *J. Am. Chem. Soc.,* **60,** 2308.
[47] Pitzer K.S. and Scott D.W., 1943. *J. Am. Chem. Soc.,* **65,** 803.
[48] Forziati A.F., Norris W.R. and Rossini F.D., 1949. *J. Re.s Natl. Bur. Stan.,* **43,** 555.
[49] NIST Chemistry Web Book, SRD 69, USA (https://webbook.nist.gov).
[50] Patterson D., 1994. *J. Solut. Chem.,* **23,** 105.
[51] Yang C., Ma P. and Zhou Q., 2004. *J. Chem. Eng. Data,* **49,** 881.

INFORMATION FOR AUTHORS

ARTICLES

The Journal of Acoustical Society of India (JASI) is a refereed publication published quarterly by the Acoustical Society of India (ASI). JASI includes refereed articles, technical notes, letters-to-the-editor, book review and announcements of general interest to readers.

Articles may be theoretical or experimental in nature. But those which combine theoretical and experimental approaches to solve acoustics problems are particularly welcome. Technical notes, letters-to-the-editor and announcements may also be submitted. Articles must not have been published previously in other engineering or scientific journals. Articles in the following are particularly encouraged: applied acoustics, acoustical materials, active noise & vibration control, bioacoustics, communication acoustics including speech, computational acoustics, electro-acoustics and audio engineering, environmental acoustics, musical acoustics, non-linear acoustics, noise, physical acoustics, physiological and psychological acoustics, quieter technologies, room and building acoustics, structural acoustics and vibration, ultrasonics, underwater acoustics.

Authors whose articles are accepted for publication must transfer copyright of their articles to the ASI. This transfer involves publication only and does not in any way alter the author's traditional right regarding his/her articles.

PREPARATION OF MANUSCRIPTS

All manuscripts are refereed by at least two referees and are reviewed by the Publication Committee (all editors) before acceptance. Manuscripts of articles and technical notes should be submitted for review electronically to the Chief Editor by e-mail or by express mail on a disc. JASI maintains a high standard in the reviewing process and only accept papers of high quality. On acceptance, revised articles of all authors should be submitted to the Chief Editor by e-mail or by express mail.

Text of the manuscript should be double-spaced on A4 size paper, subdivided by main headings-typed in upper and lower case flush centre, with one line of space above and below and sub-headings within a section-typed in upper and lower case understood, flush left, followed by a period. Sub-sub headings should be italic. Articles should be written so that readers in different fields of acoustics can understand them easily. Manuscripts are only published if not normally exceeding twenty double-spaced text pages. If figures and illustrations are included then normally they should be restricted to no more than twelve-fifteen.

The first page of manuscripts should include on separate lines, the title of article, the names, of authors, affiliations and mailing addresses of authors in upper and lowers case. Do not include the author's title, position or degrees. Give an adequate post office address including pin or other postal code and the name of the city. An abstract of not more than 200 words should be included with each article. References should be numbered consecutively throughout the article with the number appearing as a superscript at the end of the sentence unless such placement causes ambiguity. The references should be grouped together, double spaced at the end of the article on a separate page. Footnotes are discouraged. Abbreviations and special terms must be defined if used.

EQUATIONS

Mathematical expressions should be typewritten as completely as possible. Equation should be numbered consecutively throughout the body of the article at the right hand margin in parentheses. Use letters and numbers for any equations in an appendix: Appendix A: (A1, (A2), etc. Equation numbers in the running text should be enclosed in parentheses, i.e., Eq. (1), Eqs. (1a) and (2a). Figures should be referred to as Fig. 1, Fig. 2, etc. Reference to table is in full: Table 1, Table 2, etc. Metric units should be used: the preferred from of metric unit is the System International (SI).

REFERENCES

The order and style of information differs slightly between periodical and book references and between published and unpublished references, depending on the available publication entries. A few examples are shown below.

Periodicals:

[1] S.R. Pride and M.W. Haartsen, 1996. Electroseismic wave properties, *J. Acoust. Soc. Am.*, **100** (3), 1301-1315.

[2] S.-H. Kim and I. Lee, 1996. Aeroelastic analysis of a flexible airfoil with free play non-linearity, *J. Sound Vib.*, **193** (4), 823-846.

Books:

[1] E.S. Skudzryk, 1968. *Simple and Comlex Vibratory Systems*, the Pennsylvania State University Press, London.

[2] E.H. Dowell, 1975. *Aeroelasticity of plates and shells*, Nordhoff, Leyden.

Others:

[1] J.N. Yang and A. Akbarpour, 1987. Technical Report NCEER-87-0007, Instantaneous Optimal Control Law For Tall Buildings Under Seismic Excitations.

SUMISSIONS

All materials from authors should be submitted in electronic form to the JASI Chief Editor: B. Chakraborty, CSIR - National Institute of Oceanography, Dona Paula, Goa-403 004, Tel: +91.832.2450.318, Fax: +91.832.2450.602,(e-mail: bishwajit@nio.org) For the item to be published in a given issue of a journal, the manuscript must reach the Chief Editor at least twelve week before the publication date.

SUMISSION OF ACCEPTED MANUSCRIPT

On acceptance, revised articles should be submitted in electronic form to the JASI Chief Editor (bishwajit@nio.org)